Contents lists available at ScienceDirect

Remote Sensing of Environment

journal homepage: http://ees.elsevier.com

Enhanced burn severity estimation using fine resolution ET and MESMA fraction images with machine learning algorithm

Carmen Quintano [a,b,c,*], Alfonso Fernández-Manso [c,d], Dar A. Roberts [c]

[a] Electronic Technology Department, University of Valladolid, C/Francisco Mendizábal, s/n, 47014 Valladolid, Spain
[b] Sustainable Forest Management Research Institute, University of Valladolid-Spanish National Institute for Agricultural and Food Research and Technology, Spain
[c] Department of Geography, University of California, Santa Barbara, CA 93106, United States
[d] Agrarian Science and Engineering Department, University of León, Av. Astorga s/n. 24400 Ponferrada, Spain

ARTICLE INFO

Edited by Marie Weiss

Keywords
Evapotranspiration
Energy balance
MESMA
Burn severity
Random forest

ABSTRACT

Successful post-fire management depends on accurate burn severity maps that are increasingly derived from satellite data, replacing field-based estimates. Post-fire vegetation and soil changes, besides modifying the reflected and emitted radiation recorded by sensors onboard satellites, strongly alters water balance in the fire affected area. While fire-induced spectral changes can be well represented by fraction images from Multiple Endmember Spectral Mixture Analysis (MESMA), changes in water balance are mainly registered by evapotranspiration (ET). As both types of variables have a clear physical meaning, they can be easily understood in terms of burn severity, providing a clear advantage compared to widely-used spectral indices. In this research work, we evaluate the potential of Landsat-derived ET to estimate burn severity, together with MESMA derived Sentinel-2 fraction images and important environment variables (pre-fire vegetation, climate, topography). In this study, we use the random forest (RF) classifier, which provides information on variable importance allowing us to identify the combination of input variables that provided the most accurate estimate. Our study area is located in Central Portugal, where a mega-fire burned >450 km^2 from 17 to 24 June 2017. We used the official burn severity map as ground reference. The RF algorithm identified ET as the most important variable in the burn severity model, followed by MESMA char fractions. When both ET and MESMA char fraction image were used as RF inputs, burn severity estimates reached higher accuracy than if only one of them was used, which suggests their potential synergetic interaction. In particular, when environmental variables were used in addition to ET and char fraction, the highest accuracy for burn severity was reached ($\kappa = 0.79$). Our main conclusion is that post-fire fine resolution ET is a useful and easily understandable indicator of burn severity in Mediterranean ecosystems, in particular when used in combination with a MESMA char fraction image. This novel approach to estimate burn severity may help to develop successful post-fire management strategies not only in Mediterranean ecosystems but also in other ecosystems, due to ease of generalization.

1. Introduction

Wildfire causes important socioeconomic and ecological changes in forest ecosystems (Pausas et al., 2008). Forest fires remove vegetation cover increasing soil erosion (Shakesby, 2011). Furthermore, vegetation structure, composition and regeneration dynamics may be modified (Calvo et al., 2008; González-de Vega et al., 2018). Knowledge of the different levels in which fire affects an ecosystem is a key factor for a successful post-fire strategy that promotes natural regrowth, and prevents soil erosion (Lentile et al., 2006). Thus, accurate post-fire burn severity estimates are a critical tool for forest managers (Key and Benson, 2006), including both short and long-term effects (Jain et al., 2004).

Remote sensing provides an affordable alternative to field measures to obtain reliable burn severity estimates at short and long time scales, in particular when fire affects large and topographically complex areas (Pérez-Cabello et al., 2009). A large amount of research focused on the analysis of fire damage is based on remotely sensed data. Most of this research uses Landsat data (Epting et al., 2005; Mitsopoulos et al., 2019; Soverel et al., 2010; Stambaugh et al., 2015), although an increasing number of them are based on Sentinel-2 MSI data (Amos et al., 2019; O. Fernández-Manso et al., 2016; A. Fernández-Manso et al., 2016, García-Llamas et al., 2019a; Mallinis et al., 2017). Spectral indices,

* Corresponding author at: Electronic Technology Department, University of Valladolid, C/Francisco Mendizábal, s/n, 47014 Valladolid, Spain.
E-mail address: carmen.quintano@uva.es (C. Quintano)

https://doi.org/10.1016/j.rse.2020.111815
Received 29 November 2019; Received in revised form 1 April 2020; Accepted 3 April 2020
Available online xxx
0034-4257/

specifically differenced Normalized Burn Ratio (dNBR) and its derivatives are the basis of most of these studies (e.g. Hudak et al., 2007; Key and Benson, 2006; Miller et al., 2009; Miller and Thode, 2007; Soverel et al., 2010). However, other authors (Lewis et al., 2017; Roy et al., 2006) have called attention to limitations of these indices: (see Lentile et al., 2009 for a detailed explanation).

Fraction images, in particular the char fraction image, are an effective alternative to spectral indices in fire damage studies (Lentile et al., 2006; Lewis et al., 2012; Tane et al., 2018; Veraverbeke and Hook, 2013). The key to their success is the mixture of dead and remnant vegetation, burned soil and ash that typically defines the conditions of the short-term post-fire scene (Meng et al., 2017; Quintano et al., 2013). Additional advantages are: 1) fraction images are easier to interpret than spectral indices due to their physical meaning (Quintano et al., 2012), 2) they are typically derived using all spectral bands instead of just two or three bands (Veraverbeke et al., 2018) and, 3) they do not require calibration to field data (Somers et al., 2012). Typically fraction images are obtained by using spectral mixture analysis (SMA, Shimabukuro and Smith, 1991). In SMA, each pixel of an image is modeled as a linear combination of endmembers (spectra of pure components present in the scene), weighted by the abundance of the endmember in the pixel (Roberts et al., 1993). Although previous studies have shown that SMA based fraction images outperform spectral indices for fire damage assessment (Fernández-Manso et al., 2009; Lentile et al., 2006, 2009; Quintano et al., 2006), SMA does not account for endmember variability (i.e. different spectra could correspond to the same material) (Somers et al., 2011). Conversely, multiple endmember SMA (MESMA, Roberts et al., 1998) was designed to account for this endmember variability by using different spectra for each endmember class. Fraction images based on MESMA have already demonstrated their usefulness to estimate burn severity from satellite data (Lewis et al., 2017; Meng et al., 2017; Quintano et al., 2017, 2019; Tane et al., 2018; Veraverbeke et al., 2014).

In addition to modifying reflected and emitted radiation captured by sensors onboard of satellites, vegetation changes due to wildfires also alter evapotranspiration (ET, latent heat flux) (Atchley et al., 2018; Fang et al., 2018; Lentile et al., 2006; Montes-Helu et al., 2009). All of the variables of the energy balance equation, and particularly latent heat flux, are affected by the alterations in vegetation (both structure and species composition) due to wildfires (Randerson et al., 2006). Immediately following fire, ET decreases, which can be observed several years after fire (e.g. Atchley et al., 2018; Clark et al., 2012; Häusler et al., 2018; Li et al., 2018b; Rocha and Shaver, 2011; Roche et al., 2018; Sánchez et al., 2015). Variations in ET directly affect water balance (Cai et al., 2019), climate (Ellison et al., 2017) and hydrological and biogeochemical cycles (Alkama and Cescatti, 2016, Li et al., 2018a). Surface energy balance based models are the most widely used alternative to estimate ET from remotely sensed data (de la Fuente-Sáiz et al., 2017); in particular Mapping EvapoTranspiration at high Resolution with Internalized Calibration model (METRIC, Allen et al., 2007). However, very few algorithms are able to estimate ET at fine spatial resolution due to the large quantity of parameters required to achieve an adequate accuracy (van der Tol and Norberto-Parodi, 2011). Some examples are: the Earth Engine Evapotranspiration Flux (EEFlux) model (based on METRIC), and designed and implemented on the Google Earth Engine (GEE) platform (Allen et al., 2015) or the Simplified Two-Source Energy Balance (STSEB) model proposed by Sánchez et al. (2008). In this context, ET is a fundamental variable of ECOsystem Spaceborne Thermal Radiometer Experiment on Space Station (ECOSTRESS) mission (Fisher et al., 2014, 2017), although currently it only records data over the conterminous United States (CONUS) and key biomes and agricultural zones with selected FLUXNET (Baldocchi et al., 2001) validation sites.

Burn severity is also influenced by pre-fire vegetation structural parameters such as tree density and size, canopy cover, and fine fuel accumulations (Kuenzi et al., 2008; Lentile et al., 2006). Different studies about drivers of fire severity highlighted the influence of topography, weather and pre-fire vegetation characteristics (e.g. Agee and Skinner, 2005; Dillon et al., 2011; Estes et al., 2017; Fang et al., 2018; Kane et al., 2015; Storey et al., 2016). Despite the important effect of these drivers on burn severity, there are few studies that use them as additional information to complement the spectral information from satellite data to quantify burn severity. However, these factors may characterize different aspects of changes due to fire (Parks et al., 2019). Burn severity models that include different potential factors are likely to provide more relevant and accurate characterization of burn severity (Parks et al., 2019). In this context, Fernández-Manso et al. (2019) accurately modeled burn severity from MESMA fraction images, and showed that topographic and pre-fire vegetation information contributed around 25% to the final burn severity model.

Fire damage assessments may be improved using machine learning models instead of parametric ones, as they can include multiple factors as input variables (Parks et al., 2019). Accordingly, random forest (RF) (Breiman, 2001) is the classifier chosen to estimate burn severity in our study. Non-parametric supervised classifiers (RF is one of them) show a higher efficiency and accuracy than parametric classifiers (Mather and Tso, 2016). RF is being increasingly used in remote sensing applications (Belgiu and Drăguţ, 2016). Since its proposal in 2001, RF has shown its high performance as classifier in many studies on land use/land cover mapping (e.g. Camargo et al., 2019; Gislason et al., 2006; Mellor et al., 2015; Rodriguez-Galiano et al., 2012; Wang et al., 2019), tree species/plant species/crops classification (Mahdianpari et al., 2017; Naidoo et al., 2012; Teluguntla et al., 2018), and forest parameter estimation (Ahmed et al., 2015; Hudak et al., 2008). Some studies have used RF to map wildfire damage as well (e.g. Collins et al., 2018; Hultquist et al., 2014; Meddens et al., 2016; Ramo and Chuvieco, 2017). RF is based on a large number of decision trees and includes bootstrap aggregation (bagging). The combination of multiple trees increases its predictive capacity and bagging prevents overfitting usually present in a single tree (Cutler et al., 2007). Advantages of the RF algorithm can be summarized highlighting its short calculation time, its powerful performance in different applications, and the information provided about the input variables importance and the accuracy in the classification process (Rodriguez-Galiano et al., 2012; Wang et al., 2019). Additionally, RF provides information about the relevance of input variables in the classification process.

Our study aims to estimate burn severity from post-fire Sentinel-2 MESMA fractions, fine spatial resolution-ET and environmental variables, testing which combination of these input variables leads to the estimate with highest accuracy. For the first time to our knowledge the performance of ET in mapping burn severity is being tested. Our hypothesis is that the combination of ET and char fraction image is synergetic and that a higher accuracy can be achieved than these variables are used individually. Fraction images would reflect the spectral change that fire causes, and ET provides information on water balance alteration. Specifically, our research questions can be summarized as: 1) Can an accurate burn severity estimate be obtained from post-fire fine spatial resolution ET?; 2) If yes, what would be the relative importance of post-fire ET versus post-fire MESMA char fraction when used together to estimate burn severity?; and 3) What would be the relative importance of environmental

variables (in particular: pre-fire vegetation, climatic and topographic variables) to estimate burn severity when used together to post-fire ET and MESMA fractions?

2. Study area and materials

2.1. Study area

We studied the Pedrogão Grande mega-fire in central Portugal. This fire burned 458.93 km2 between the 17th and 24th of June 2017 (ADAI/LAETA, 2017) (Fig. 1). Due to the high loss of lives (66), injuries (>200) and buildings (263) (Ribeiro et al., 2018), Pedrogão Grande mega-fire was included in the annual report of the Joint Research Centre of the European Commission (San-Miguel-Ayanz et al., 2018). On the day of ignition (17th June 2017), almost all of the region was in severe drought as declared by the Instituto Português do Mar e da Atmosfera (IPMA) (www.ipma.pt).

The study area is located in the transition zone between typical and humid Mediterranean Köppen-Geiger climatic classes (Köppen, 1936). The typical Mediterranean (Csa class) has rainy winters and hot and dry summers. It's annual precipitation ranges from 400 to 750 mm, whereas the humid Mediterranean (Csb class) displays higher annual precipitation (from 750 to 2000 mm) and milder summers (see Fig. 1, left upper). Elevation varies from slightly >1000 m in the north and northwest of the affected area to 100 m on the banks of the Zêzere River, although moderate elevations (approximately 400 m) predominate around Pedrógão Grande (see Fig. 1, right lower). Similarly, the north and northeast areas have steep slopes (around 40%–60%), whereas the areas in the Basin of Zêzere River are flatter (0%–15% slope) (see Fig. 1, right lower). Pedrógão Grande and the surrounding counties affected by fire are included in the Interior North Pinhal Zone, the largest European forest before the fire. Plantations of Eucalyptus blue gum (*Eucalyptus globulus* Labill.), and pine forest (*Pinus pinaster* Ait.) are the dominant vegetation. Other vegetation in the region includes the chestnut (*Castanea sativa* Mill.), cork oak forests (*Quercus suber* L.) and strawberry trees (*Arbutus unedo* L.). Shrubs consisted mainly of red heather (*Erica aus-*

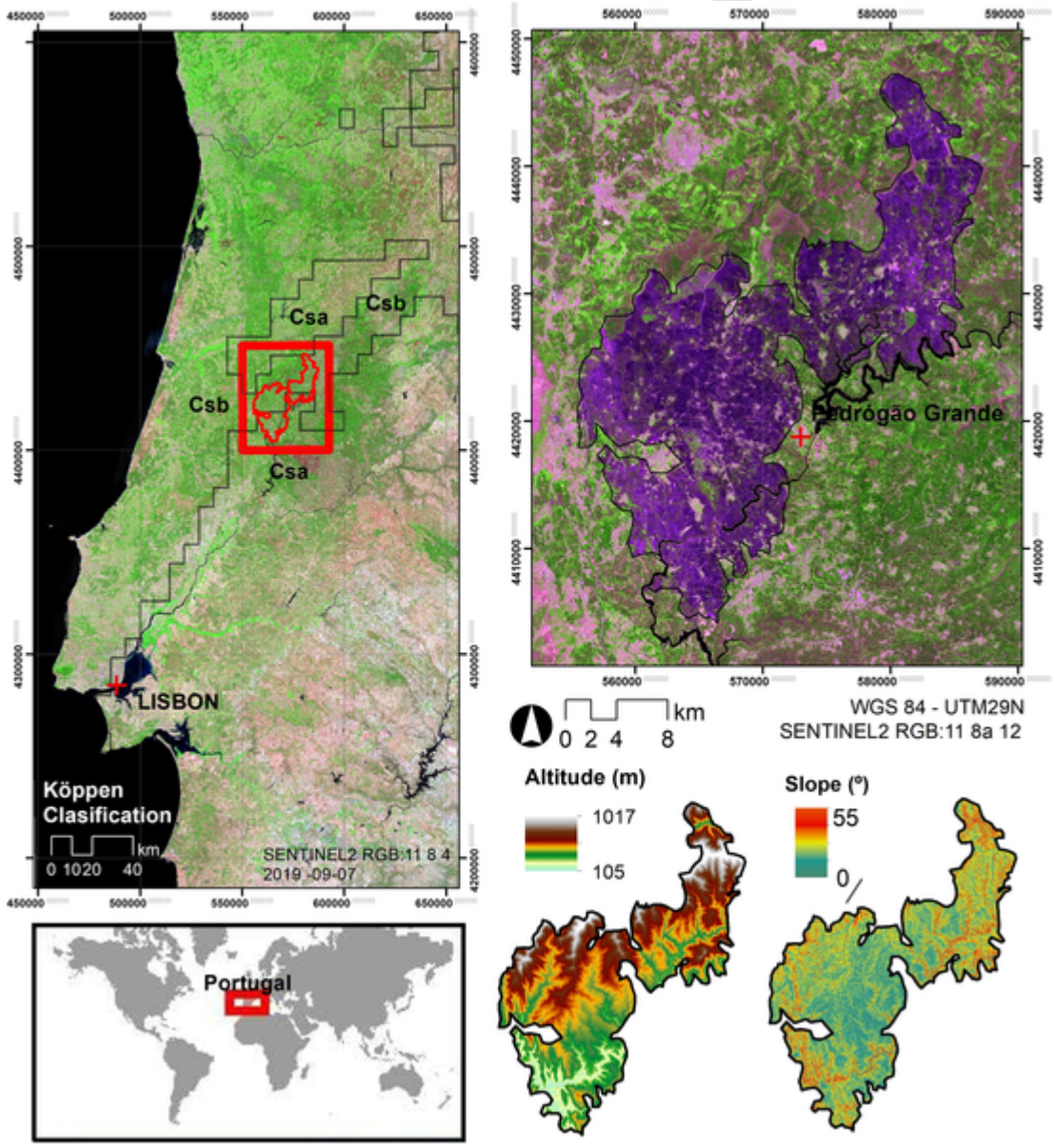

Fig. 1. Location of study area. Left: Köppen climatic classes (upper), and location in world map (lower); right: post-fire Sentinel 2 color composite RGB: 11 8a 12 (upper), and altitude and slope maps (lower).

tralis L.), white heather (*Erica arborea* L.), gorse (*Ulex europaeus* L.), and broom (*Cytisus scoparius* L.). Some small agricultural lands are situated close to villages (CTI, 2017).

2.2. Materials

Fraction images were calculated from a post-fire Sentinel-2 Multispectral Instrument (MSI) image acquired on 4th July 2017 that was downloaded from Copernicus Open access Hub. This image was the closest to the fire event without clouds. It had a processing level 2A, producing bottom-of-atmosphere reflectance in UTM/WGS84 projection (ESA, 2015). Only one tile was needed to cover the study area. We resampled the visible spectral bands to a spatial resolution of 20 m by using the nearest neighbor resampling algorithm of the Sentinel-2 Toolbox integrated on Sentinel Application Platform (SNAP) provided by the European Spatial Agency (ESA). A post-fire daily ET image of 1st July 2017 with a spatial resolution of 30 m was obtained from University of Nebraska-Lincoln (EEFlux application Allen et al., 2015).

Pre-fire vegetation was characterized by using fuel model and tree cover density (TCD) maps. The fuel model map was provided by the Instituto da Conservação da Naturaleza e das Florestas (Nature and Forest Conservation Institute) of Portugal (http://www2.icnf.pt/portal/florestas/dfci/cartografia-dfci). It was based on the Northern Forest Fire Laboratory (NFFL) fuel model and on the national fuel model linked to the Farsite code, using the official Portuguese Land Cover Map (Carta de Ocupação do Solo, COS15) as cartographical base: a minimum cartographic unit of 1 ha and a minimum distance between lines of 20 m (DGT, 2018). For TCD, we used the High Resolution Layer Forest layer provided by the Copernicus Land Monitoring Service (CLMS), coordinated by the European Environment Agency (EEA). This layer is based mainly on Sentinel-2A data from ESA as well as Landsat 8 data from the United States Geological Survey (USGS) for the 2015 year and has a spatial resolution of 20 m. We assumed that only small changes in cover density happened in the study area between 2015 and 2017. The TCD layer was compared to a 50 cm 2015 orthophotograph provided by the Portuguese Directorate General for the Territory and the Agriculture and Fisheries Finance Institute. Very high concordance between both of them was observed.

Climate was characterized by using the Köppen-Geiger climatic classes (Köppen, 1936). In our study, the climatic classes were extracted from the updated world map of the Köppen-Geiger climate classification (Peel et al., 2007). Thus, the Köppen-Geiger map had a spatial resolution of 5 arc minutes (~ 7.75 km) (Rubel et al. (2017), that is fine enough to distinguish the two climatic classes of the study area. Finally, we used a 30 m Advanced Spaceborne Thermal Emission and Reflection Radiometer (ASTER) Global Digital Elevation Model Version 2 (GDEM V2) provided by USGS (https://search.earthdata.nasa.gov) to calculate the three topographic variables (elevation, aspect and slope) used in the study.

The Portuguese Study Center of Forest Fires provided the official burn severity (three severity levels) and fire perimeter maps that were used as ground reference. They were based, respectively, on the grading map and fire perimeter map distributed by the Copernicus - Emergency Management Service of the European Union, and were built using SPOT 6 and 7 imagery. The Portuguese Study Center of Forest Fires verified them and corrected some mistakes (especially in the north of the burned area, and in unburned areas within the fire perimeter). Its work was based on fieldwork and photointerpretation of Sentinel 2 MSI data. Their estimated geometric accuracy is 5 m CE90 or better (ADAI/LAETA, 2017). Those maps helped as well to define spectra of char endmember; although we mainly relied on a post-fire SPOT 7 image acquired on 21st June 2017 to build the spectra library required by the MESMA procedure. COS15 also assisted us in digitizing polygons over the SPOT 7 image to obtain spectra of vegetation endmember.

3. Methods

We used a RF classifier to estimate burn severity while analyzing the contribution of each input variable to the final estimation. We tried different input databases: 1) post-fire char fraction, pre-fire vegetation, climatic and topographic variables; 2) post-fire ET, pre-fire vegetation, climatic and topographic variables; 3) post-fire char fraction, post-fire ET, pre-fire vegetation, climatic and topographic variables; 4) post-fire char fraction and post-fire ET.

3.1. RF input variables

Three main steps are distinguished in the MESMA procedure used to obtain the fraction images: 1) spectral library building; 2) spectral library optimization; and 3) spectral unmixing. A spectral library used to unmix an image should include the different land covers present in the study area (Roberts et al., 1998). Endmember spectra to form our spectral library may be extracted from the image to be unmixed (image endmembers) or from an external spectral library that may include spectra obtained from the field, other images or laboratory (reference endmembers). However, an accurate endmember definition is key factor for a successful unmixing (Tompkins et al., 1997). In our study, image endmembers were used to build the spectral library (Fernández-Manso et al., 2012; Quintano et al., 2017) to unmix the post-fire Sentinel-2 MSI image. As in previous studies (Quintano et al., 2013, 2017), we considered as endmembers to unmix the image: char, green vegetation (GV), non-photosynthetic vegetation (NPV), soil, and shade. Because our study area includes rivers and a dam, we also included water as a endmember to minimize the potential confusion between char and water. Based on Roth et al. (2012) and Dudley et al. (2015), we delineated georeferenced polygons over the SPOT 7 image to characterize the classes included in the study with the help of the official Portuguese Land Cover Map. Char endmembers were defined from polygons inside the fire perimeter. From these polygons we obtained all of the endmembers that constituted the potential spectral library.

However, it is necessary to determine those spectra that are most representative of a particular class, and least possible to be confused with spectra from a different class (Roberts et al., 2019). We selected the optimal spectra using two approaches. The first was a semi-automatic procedure based on three indices: 1) Count-based Endmember Selection (CoB, (Roberts et al., 2003) that selects the endmembers that model the maximum quantity of endmembers within their class; 2) Endmember Average RMSE (EAR, Dennison and Roberts, 2003); that selects the endmembers that produced the minimum RMSE within a class; and 3) Minimum Average Spectral Angle (MASA, Dennison et al., 2004), that selects the endmembers that showed the minimum average spectral angle. The second procedure followed the Iterative Endmember Selection method (IES) proposed by Schaaf et al. (2011), and updated by Roth et al. (2012). IES includes (and removes) iteratively endmembers from a spectral library to a spectral library subset to maximize the classification accuracy measured by κ statistic. It is also possible to force the inclusion of rare endmembers (Roth et al., 2012).

Once the spectral library has been optimized, the input images can be unmixed. There are many unmixing possibilities depending on how the spectra are grouped. Models of different complexity (1, 2, 3, 4 or more endmembers) can be run, though 4-endmember models have been commonly used in burn severity studies (Lewis et al., 2017; Meng et al., 2017; Quintano et al., 2013, 2019), in particular: char, GV, NPV and soil (NPVS), and shade. In this work, we

enabled different levels of complexity for each pixel by using the multi-level fusion approach proposed by Roberts et al. (2003). The higher level of complexity is used when the RMSE decrease (due to the complexity increase) exceeds a threshold that was empirically fixed at 0.002. As in previous studies (O. Fernández-Manso et al., 2016; A. Fernández-Manso et al., 2016; Fernández-Manso et al., 2019), we used the following constraint values: maximum and minimum admissible fraction values, 1.10 and −0.10 respectively; minimum and maximum allowable shade fraction values, 0.00 and 0.85, respectively; and maximum allowed root mean square error (RMSE), 0.025. Additionally, the minimum number of classified pixels considered acceptable for an unmixing process to be valid was fixed at 95% of the image (Quintano et al., 2013). If this last requirement was not fulfilled, we varied the components of a model, the members of a class, and/or the level of complexity of the models and repeated the unmixing process. Finally, fraction images were shade normalized before using them as RF inputs. Shade normalization removes the contribution of the shade endmember and results in stressing the contribution of non-shade endmembers (Rogan and Franklin, 2001). All operations to unmix the Sentimel-2 post-fire image were completed by the Visualization and Image processing for Environmental Research (VIPER) tools software (Roberts et al., 2019) developed at the Department of Geography at University of California Santa Barbara (https://sites.google.com/site/ucsbviperlab/viper-tools).

A post-fire Landsat-derived daily ET image based on the EEFlux model (Allen et al., 2015) was also used as a RF input. This model is derived from the surface energy balance equation (see Allen et al., 2007; and Irmak et al., 2011, for detailed information).

$$LE = R_n - G - H \quad (1)$$

where LE is latent heat flux, expressed in W/m^2; R_n, is net radiation estimated from reflectance and LST; G, soil heat flux, estimated from R_n, LST, and vegetation indices; and H, air heat flux, estimated from LST ranges, surface roughness, and wind speed.

Instantaneous ET (ET_i, expressed in mm/h) is computed for each pixel by dividing LE by the latent heat of vaporization, which is dependent on land surface temperature. From it, daily ET is calculated by extrapolating ET_i to a 24-hour period using reference ET_i of a tall crop (alfalfa) as the reference.

Pre-fire vegetation, climatic, and topographic variables were also included as RF input variables. Four classes represented the pre-fire fuel model: 1) Pastures and meadows (<0.5 m, fine fuel load: 1–1,5 t/ha). This class is represented as "V-Hb" using the Portuguese fuel code (Fernandes et al., 2009), and corresponds to a fuel model 1 using NFFL code (Anderson, 1982); 2) Eucalyptus forest (Eucalyptus foliage with dense underbrush with a height <0.6 m, fine fuel load: 9–18 t/ha). This class is represented as "M-EUC" using the Portuguese fuel code, and corresponds to a fuel model 5 using NFFL code; 3) *Pinus pinaster* forests (Medium to long needle pine litter – 5 cm or less- with shrub understory, fine fuel load: 8–18 t/ha). This class is represented as "M-PIN" using the Portuguese fuel code, and corresponds to a fuel model 9 using NFFL code; and 4) Continuous pastures with the presence of young shrubs, (under 3 years old since last fire, height <1 m), and green shrubs, often discontinuous. This class is represented as "V-MH" using the Portuguese fuel code, and corresponds to a fuel model 2 using NFFL code. These four classes constituted 96% of area inside the fire perimeter (in particular: V-Hb: 8.42%, M-EUC: 49.56%, M-PIN: 31.99%, and V-MH: 6.51%). Two Köppen climatic classes were taken into account in the study: Csa (Mediterranean climate) and Csb (humid Mediterranean climate). Regarding topographic factors, both elevation and slope were included as continuous variables in the RF classifier, but aspect was categorized in to eight classes: North (0°-22.5° and 337.5°-360°), Northeast (22.5°-67.5°), East (67.5°-112.5°), Southeast (112.5°-157.5°), South (157.5°-202.5°), Southwest (202.5°-247.5°), West (247.5°-292.5°), and Northwest (292.5°-337.5°).

Before using these variables as RF inputs, we resampled the shade-normalized char fraction (char_sn) and the TCD to 30 m using nearest neighbor resampling. Similarly, fuel model and climatic maps were rasterized using 30 m as spatial resolution. Once all input variables had the same spatial resolution (30 m), a mean 3 × 3 filter was applied to all continuous variables (shade-normalized char fraction, ET, TCD, elevation and slope) and a mode 3 × 3 filter to every categorical variable (fuel model, climatic class, aspect) to minimize positional errors (Key and Benson, 2006). We adopted a stratified random sampling (Congalton and Green, 2009), taking a number of samples for each burn severity level related to its area on the reference map: 2357 samples for high burn severity, 1694 for moderate burn severity and 661 for low burn severity level. 1140 sampling points from the zone outside fire perimeter defined the unburned class. Correlation among all RF inputs was very low except between ET and shade-normalized char fraction (partial correlation coefficient, 0.66). This value is, however, not too high. Thus ET and char may contribute with different information to the final burn severity model.

3.2. RF based classification

Random Forest (Breiman, 2001) is a machine learning approach that builds a large number of binary decision threes that are not statistically pruned. The combination of such number of trees increases the predictive capacity and decreases overfitting usually present in a single tree (Cutler et al., 2007). Each tree is built using bootstrap aggregation (bagging), that randomly selects, with replacement, two-thirds of the input samples to train the tree (referred as in-bag samples) (Breiman, 1996). The randomness to build a tree due to bagging is complemented by the random approach used to choose a subset of input variables to define each tree split (Liaw and Wiener, 2002). The samples that are not selected are used in an internal cross-validation technique for assessing the accuracy of the final classification. As they are referred as out-of-bag (OOB) samples, a common measure of the RF accuracy is the OOB error. In RF the average vote of the trees is what determines the final result (Hastie et al., 2009). In particular, in the RF training, RF determines the final class assignment by using the arithmetic mean of the class assignment from each tree, whereas in the classification step, RF assigns to each pixel the class that achieves the majority value among the votes of every tree (Breiman, 2001).

There are two user-defined parameters needed to build random forests: number of trees to be grown and number of variables used to split a node. We fixed the number of trees at 500, as we verified that the error rate was not sensitive to the number of trees over this value. Moreover, this is the number that a majority of RF studies used (Belgiu and Drăguţ, 2016). The number of splitting variables in each node was set to its default value (the square root of the number of input variables) as previous works recommended (e.g. Gislason et al., 2006; Naidoo et al., 2012; Wang et al., 2015).

RF also provides individual variable importance. The variable importance measures the contribution of a variable in the final model, enabling the identification of the variable or set of variables most relevant for the final classification. Most of studies based on RF evaluated the importance of each variable by measuring the reduction in accuracy observed (increase in OOB error), when the observed values of this variable are randomly exchanged in the OOB samples (Belgiu and Drăguţ (2016). Mean decrease in Gini index, a measure of node impurity, is another alternative (Schmidt et al., 2014). In our study, the relative importance of each variable was

measured by the mean decrease in accuracy criterion. Specifically, OOB error is computed for each tree. After permuting each variable the OOB error is calculated again. Next, the difference between these two OOB error values is averaged over all trees, and, finally, normalized by the standard deviation of the differences (Breiman, 2001). The most important variables reach higher decrease in accuracy.

Another important advantage of using RF classification is that availability of OOB error may omit the requirement for a post-classification accuracy assessment (Chrysafis et al., 2017; Lawrence et al., 2006; Zhong et al., 2014). Rodriguez-Galiano et al. (2012) highlighted that each tree has a different subset of OOB samples, and that the OOB samples that were not used for training of the tree are classified to provide a measure of the RF performance. In our study, the RF classifier had a relative high number of initial samples. Consequently, we decided to assess the classification accuracy by the OOB samples exclusively. Confusion matrixes were calculated from them and Overall Accuracy (OA), Producer's Accuracy (PA), User's Accuracy (UA), and κ statistic were computed as well (Congalton and Green, 2009). To compare the accuracy of the obtained burn severity classifications from each input database, a Z-test based on the κ statistics was used (Congalton and Green, 2009). Note that $z_c = 1.96$ at the 95% confidence level, and that the null hypothesis H0: $(\kappa 1\text{-}\kappa 2) = 0$ is rejected when $Z > z_c$. XLSTAT v.19.3.2 software (Addinsoft, 2019) together to Scikit-learn v0.21.3 (Pedregosa et al., 2011) were used to implement the RF classifier and obtain the graphical outputs.

4. Results

After different trials varying the hierarchical level of spectral library, the endmember optimization approach and the model complexity, we achieved adequate post-fire Sentinel-2 MSI fraction images. Three hierarchical levels were established in the spectral library. The level 3 classified the highest percentage of pixels of Sentinel-2 MSI image. However, slight differences were found using the level 2. The hierarchical level 3 grouped NPV, soil and water in just one category NPVSW, with the other two categories consisting of GV and char at this level. Table 1 summarizes the hierarchical structure of the spectral library used. The semi-automatic approach based on CoB, EAR and MASA indices (EMC approach) was finally used to unmix the post-fire image as it classified a higher number of pixels than the IES-based approach, although the difference was not very large. Multi-level fusion was used in this work. Thus, models with different levels of complexity may unmix each pixel of the inputs images. In particular, we used 44 2-endmember models, 569 3-endmember models and 2376 4-endmeber models to unmix the post-fire image. Table 1 includes a summary of the unmixing results, showing how many pixels of the image were unmixed by models of 2-, 3- and 4- endmembers, respectively.

Fig. 2 shows the shade-normalized fraction images derived from the MESMA procedure. Char and GV fraction images (Fig. 2, left and center) clearly discriminate burned form unburned areas, while level differences within the burned area suggest differences in burn severity levels. In the shade-normalized NPVSW fraction, the Zêzere River is evident although there is some confusion with the char fraction. Examples of the endmember spectra used to unmix the Sentinel-2 are also included in Fig. 2. Fig. 3 compares (comprising both burned and unburned areas) RGB color composites of the shade normalized fraction images and of the visible bands of SPOT 7 image used to identify the endmembers for four locations. We observed a high level of agreement between both RGB compositions in all locations; burned areas are clearly and correctly identified. Additionally, from locations 1 and 2 we observed how MESMA fraction images clearly distinguished the main road and the small villages, from the burned and unburned areas. In location 3, discrimination of the Zêzere River, in particular of the Cabril dam, can be observed in both RGB color compositions. Finally, location 4 also revealed the identification of the main river (Castelo de Bode dam) and small villages. Similarly clear differences between burned and unburned areas in the immediately post-fire ET image are evident (Fig. 4). The

Table 1
Hierarchical levels of MESMA spectral library and summary of unmixing results.

Hierarchical levels of spectral library		
Level 1	Level 2	Level 3
Eucalyptus globulus Labill. *Pinus pinaster* Ait. *Quercus suber* L. *Castanea sativa* Mill.	GV	GV
Non irrigated lands Dry grasslands Forest clearcuttings	NPV	NPVSW
Open mine Urban areas Roads	Soil	
River	Water	
High burn severity Moderate burn severity	Char	Char

Summary of unmixing results			
Model complexity	Hierarchical level 3	Post-fire image classified	
		#pixels	% over total pixels
2-endmember models	CHAR - shade	173,767	3.19
	GV – shade	462,825	8.48
	NPVSW - shade	199,220	3.65
	Total 2-endmember	**835,812**	**15.32**
3-endmember models	CHAR – GV - shade	131,447	2.40
	CHAR – NPVSW - shade	658,615	12.07
	GV - NPVSW - shade	3295,318	60.41
	Total 3-endmember	**4084,855**	**74.88**
4-endmember models	CHAR – GV – NPVSW –shade	**491,334**	**9.01**
	Total 4-endmember		
	TOTAL	**5412,001**	**99.21**

GV: green vegetation; NPV: non-photosynthetic vegetation, NPVSW: non-photosynthetic vegetation, soil and water.

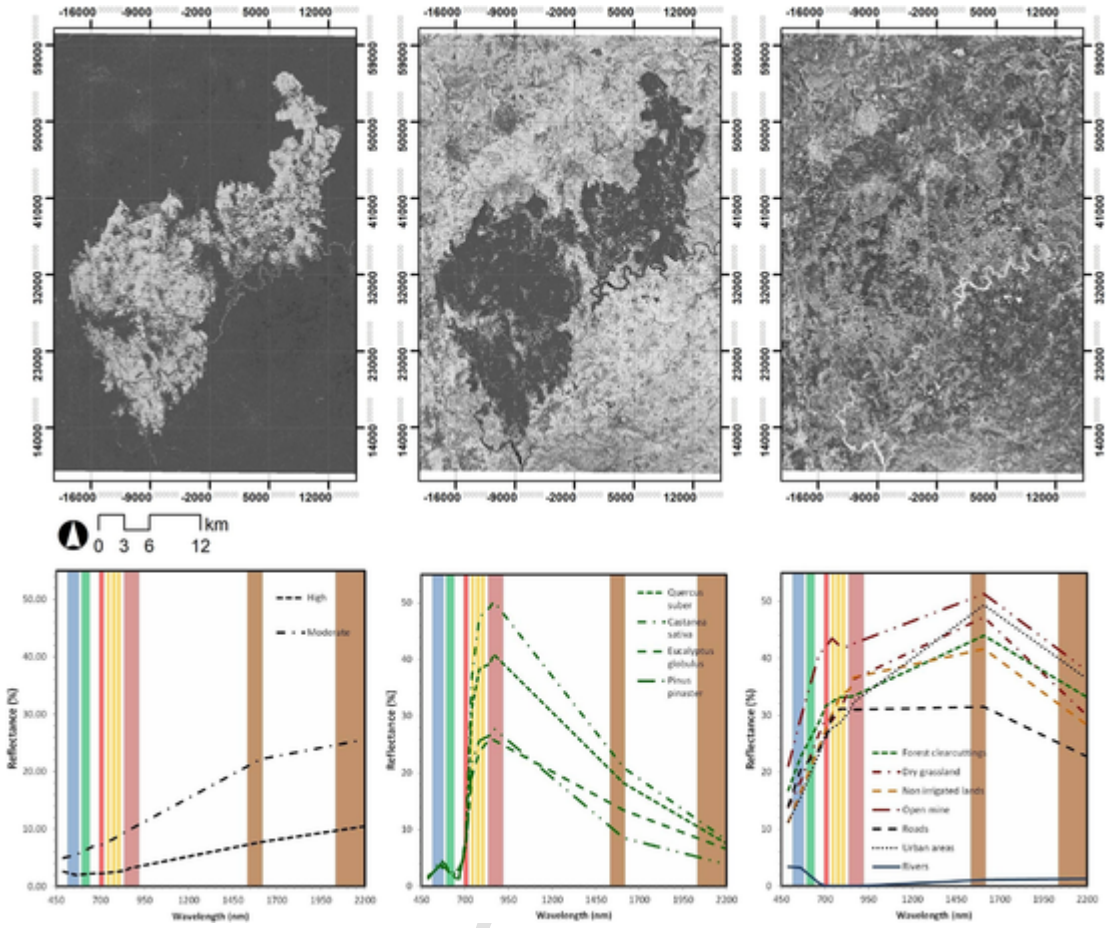

Fig. 2. Upper: Shade normalized MESMA fraction images: char (left), green vegetation (center), non-photosynthetic vegetation, soil and water (right). Lower: examples of endmember spectra used to unmix the Sentinel-2 MSI image: char (left), green vegetation (center), non-photosynthetic vegetation, soil and water (right).

post-fire ET image distinctly identified the Zêzere River with Cabril and Castelo de Bode dams. The affluent Unhais was clearly discriminated only in its last part, similarly to NPVSW fraction image. The profile over the image shows the variations in ET values inside the burned area supposedly related to burn severity.

Variables of each input database were ranked by their importance in the final classification using the mean decrease in accuracy when the variable was excluded from a classification (Table 2). Char fraction exhibited a predominant contribution when used together with the environmental variables used in this work (input database 1). Fuel model, climate class and elevation followed as the next most relevant variables. Similarly, ET was the most important variable when used solely as the input in database 2. In this case, fuel model and aspect were the next most relevant variables with similar mean decreases in accuracy values, followed by climate class, elevation and slope. When all of the variables tested in this study were used (input data base 3), ET was the variable that most contributed to the final model, followed by the char fraction image. Fuel model, climate class elevation and aspect, also had a noticeable contribution though not so relevant as ET and char. ET also had a higher importance than char fraction when only these two variables were used as inputs (input database 4), though the relative importance of char fraction increased versus its relative importance when input database 3 was used.

Fig. 5 displays the importance of each variable in the final classification of each burn severity level, when all the input variables were used (input data base 3). From this figure, it is evident that the char fraction contributed more to classification of the high burn severity level than to low and moderate levels. Conversely, ET helped most to discriminate unburned areas, although its importance for classifying the high burn severity level was also appreciable. Fuel model also showed relatively high importance distinguishing high and low burn severity levels.

Accuracy parameters based on the confusion matrices provided by the RF classifier are displayed in Table 3. κ statistic of burn severity estimates using the input databases 1 and 2 were quite similar ($\kappa = 0.72$ and $\kappa = 0.71$, respectively), and the Z-test based on their κ statistics showed no statistically significant difference between these two model inputs ($Z = 0.43 < 1.96$). Burn severity estimate based on input database 3 showed the highest κ statistic value ($\kappa = 0.79$) followed by the estimate from input database 4 ($\kappa = 0.76$). Classifications based on databases 1 and 2 were statistically significantly different from classifications based on input databases 3 and 4. Similarly, the Z-test showed there was statistical differences between κ statistic values of the classifications from input databases 3 and 4 ($Z = 1.99 > 1.96$). Regarding PA and UA values for each burn severity class, the low burn severity level had the lowest values. Unburned and high burn severity classes reached the higher values, and the moderate level displayed medium values. The burn severity map based on the RF classification with the highest accuracy (input database 3) is included in Fig. 6.

5. Discussion

MESMA unmixed a high percentage of the Sentinel-2A image (99.21%) using char, GV, NPVSW and shade endmembers. One of the main reasons for this high value was a satisfactory endmember

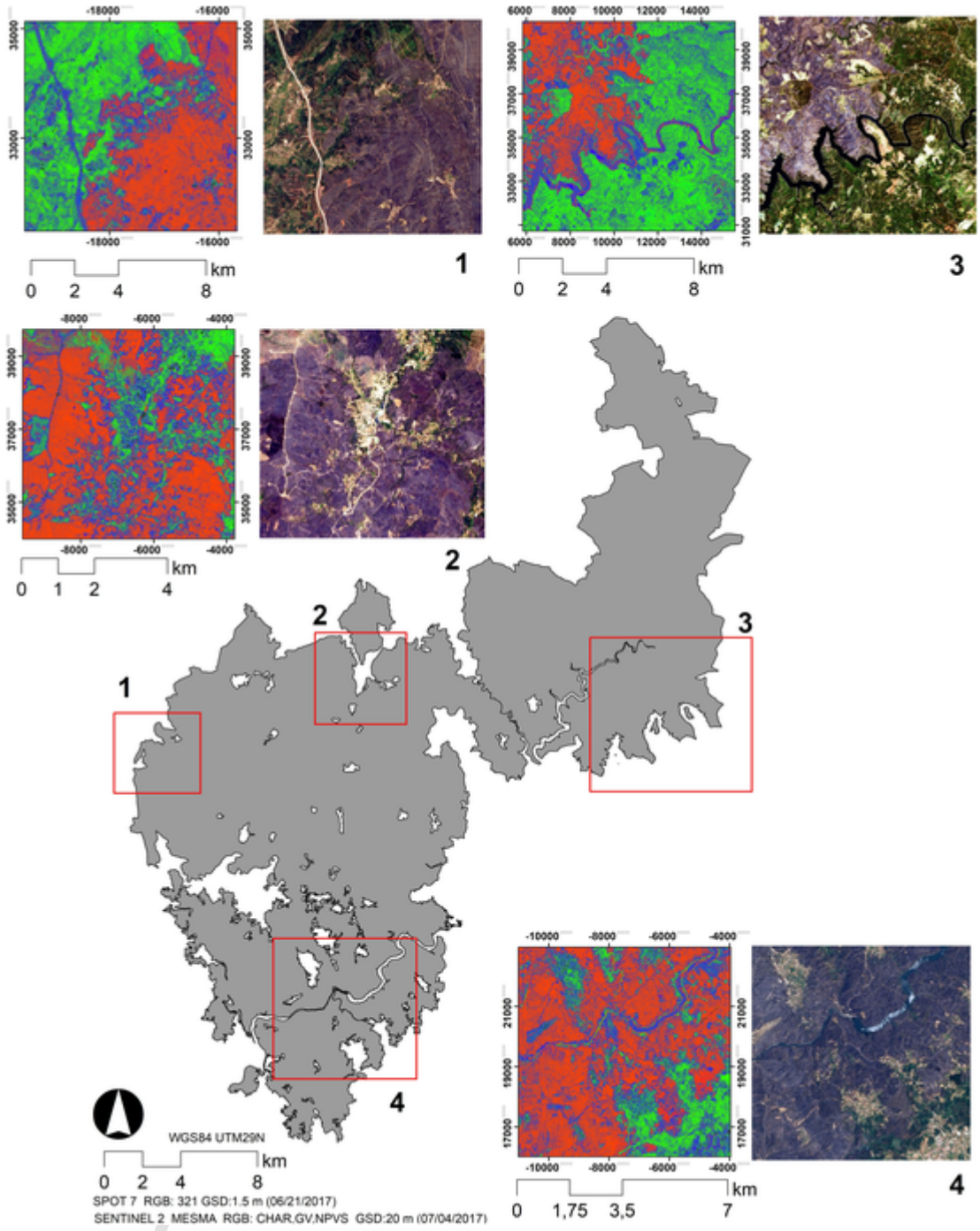

Fig. 3. Detailed comparison between RGB compositions of shade normalized MESMA fraction images (R:char, G:green vegetation, B:non-photosynthetic vegetation, soil and water) and visible bands of SPOT 7 image (R:3, G:2, B:1).

choice to build the spectral library (based on CoB, EAR and MASA indices). A slight difference in the percentage of classified pixels was found using endmembers selected by IES approach. Similarly, some MESMA based studies (Dennison et al., 2019; He et al., 2019; Quintano et al., 2013, 2019) have successfully used CoB, EAR and MASA indices to define the final endmembers, whereas others (Quintano et al., 2017; Roberts et al., 2012, 2017) used the IES procedure. In our study, NPV, soil and water formed just one category (NPVSW), in the hierarchical level 3 of the spectral library finally used to unmix the Sentinel-2A image. GV and char were the other two categories. This pattern of endmember grouping was also used in previous fire damage studies based on MESMA (Fernández-Manso et al., 2019; Quintano et al., 2019).

RF ranked the importance of the different tested variables to model burn severity. Char fraction showed the maximum importance when using the input database 1 (char_sn, fuel model, TCD, climate, elevation, slope and aspect), particularly in unburned and high burn severity classes. Burn severity estimation from database 1 (that mainly relied on MESMA char fraction) had a moderate-high level of accuracy ($\kappa = 0.72$). That result agrees with previous studies (Fernández-Manso et al., 2009; Lentile et al., 2006, 2009; Veraverbeke and Hook, 2013) that proved that reliable burn severity estimates can be based on char fraction image, and more specifically

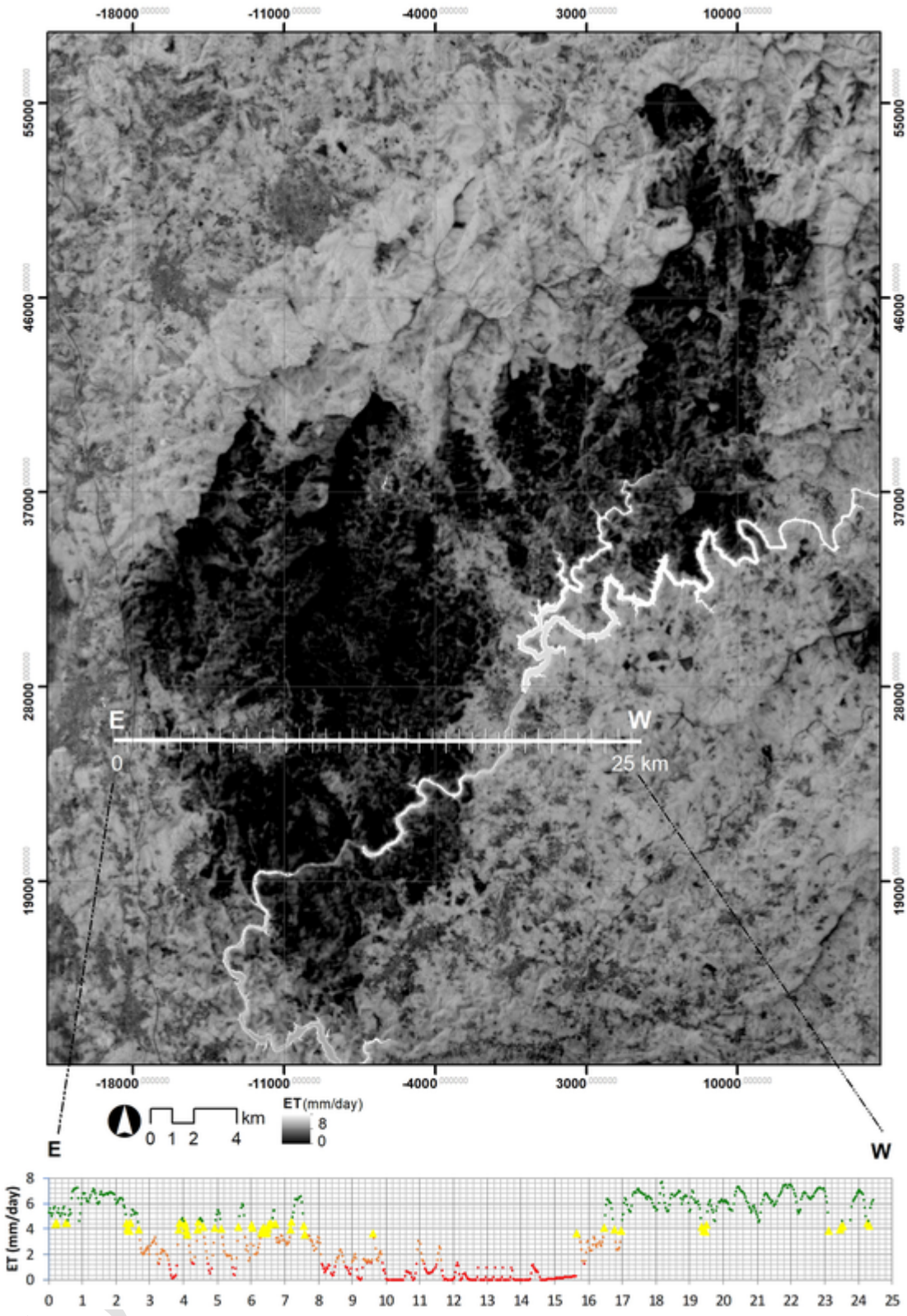

Fig. 4. Post-fire ET image with spatial profile.

on MESMA char fraction image (Fernández-Manso et al., 2019; Lewis et al., 2017; Quintano et al., 2013, 2017; Veraverbeke et al., 2014). Conversely, when char fraction was used as input together with ET (input databases 3 and 4), the char fraction was the second most important variable following ET. Burn severity estimates based on those input databases (including both char fraction image and ET as variables) displayed the highest accuracy level. When the input database included ET but not char fraction (input database 2) burn severity estimate reached similar accuracy than the burn severity estimate based on input database 1 ($\kappa = 0.71$). These

Table 2
Variable importance in the final classification represented by the mean decrease in accuracy when the variable is excluded of a classification.

Variables	Input database 1		Input database 2		Input database 3		Input database 4	
	μ	σ	μ	σ	μ	σ	μ	σ
Char_sn	172.87	0.001	–	–	53.53	0.001	56.06	0.002
ET	–	–	266.60	0.001	165.41	0.002	124.94	0.002
Fuel model	24.81	0.001	21.69	0.001	19.54	0.001	–	–
TCD	11.60	0.001	2.94	0.002	4.10	0.001	–	–
Climate	23.11	0.001	14.40	0.003	17.26	0.000	–	–
Elevation	25.93	0.000	13.90	0.001	12.09	0.000	–	–
Slope	5.28	0.001	12.63	0.001	6.87	0.001	–	–
Aspect	8.97	0.001	23.79	0.001	14.15	0.000	–	–

μ: mean value; σ: standard deviation; Char_sn: shade normalized char fraction; ET: evapotranspiration; TCD: tree cover density; input data base 1: char_sn, fuel model, TCD, climate, elevation, slope and aspect; input data base 2: ET, fuel model, TCD, climate, elevation, slope and aspect; input data base 3: char_sn, ET, fuel model, TCD, climate, elevation, slope and aspect; input data base 4: char_sn, ET.

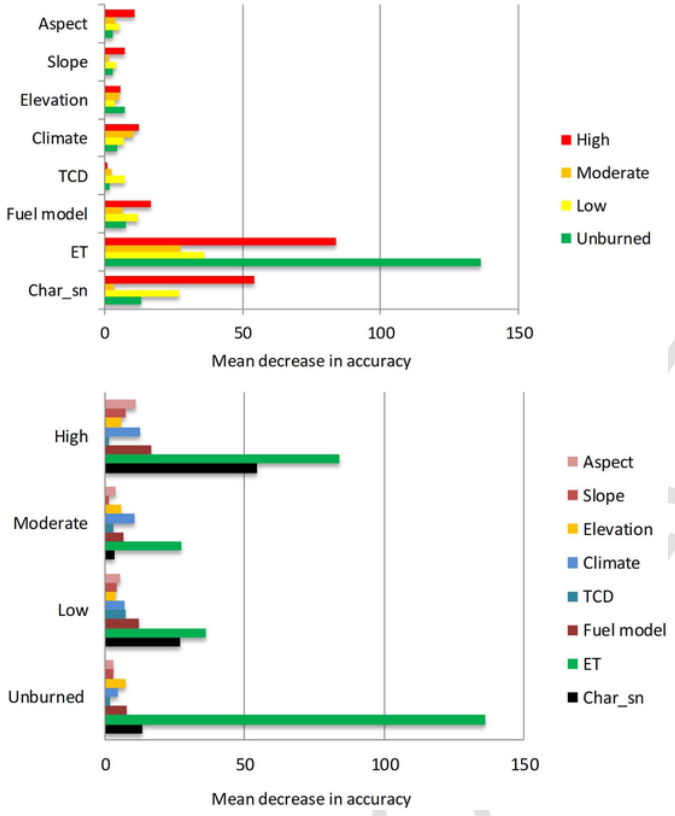

Fig. 5. Variable importance in each burn severity level represented by the mean decrease in accuracy when the variable is excluded from a classification. Top: grouped by input variable; bottom: grouped by burn severity level.

facts suggest synergies between ET and char fractions to estimate burn severity. Fraction images are based on post-fire spectral information of all Sentinel-2 reflective wavelengths. They are a more scalable alternative to the standard dNBR –based method to assess burn severity (Veraverbeke and Hook, 2013). In addition, they have a more robust biophysical base and are easier to interpret than field burn severity indices as Composite Burn Index (CBI) (Lewis et al., 2017). ET contains information about water balance alteration due to fire (Cai et al., 2019). Similar to fraction images, ET has a clearly physical meaning related to fire damage. As char fraction and ET provide different information about the induced changes by fire, we suggest that they are complementary generating the highest accuracy when used in combination. There are no previous studies (to our knowledge) that use ET as a basis to model burn severity, though availability of ET at fine scale may lead to use it as an appropriate index of burn severity in the future. Different research studies have, however, shown the strong relationship between ET and fire damage showing a reduction in ET after fire (Dore et al., 2010; Poon and Kinoshita, 2018; Rocha and Shaver, 2011; Sánchez et al., 2015). Focusing on Eucalyptus dominated forests, Häusler et al. (2018) observed in an area close to our study area a strong decrease in ET immediately after a fire event (mainly in moderate and high burn severity levels) that was not noticed two years later. Nolan et al. (2014) reported as well an important decrease in ET after fire in Australian Eucalyptus forests. Similarly, in our study areas dominated by Eucalyptus and maritime pines also showed a reduction in ET after fire (see profile of Fig. 4).

Pre-fire vegetation, climate and topographic variables caused a moderate increase in accuracy of burn severity estimates (κ statistic grew from 0.76 -input database 4- to 0.79 –input database 3-). Environmental variables influence fire occurrence, development and extent, although their effect on burn severity is still unclear (Birch et al., 2015; Mitsopoulos et al., 2019). In our study, RF ranked fuel model class (associated to pre-fire vegetation characteristics) as the third most important variable, which indicates the relevance of this parameter in burn severity. Inclusion of maps of vegetation type, structure and fuel to improve burn severity estimates has been previously recommended by Dillon et al. (2011). Both composition and structure of pre-fire vegetation (linked in fuel model class) are an important bottom-up control of fire severity (Estes et al., 2017). For that reason, fuel is increasingly viewed as a relevant factor among environmental controls of fire severity (Kraaij et al., 2018). As summarized by García-Llamas et al. (2019b), fuel structure and moisture influence fire spread and behavior, which mainly regulates fire severity (Harris and Taylor, 2017). Fuel amount and composition (directly related to fuel model) alter heat flux of the burning process, which largely influences the spatial structure of fire severity (Fang et al., 2018). Some studies (Kraaij et al., 2018; Lydersen et al., 2017) showed that burn severity was clear linked to fuel attributes, in particular in low severity regimes (Finney et al., 2005). Other studies (Dillon et al., 2011; Estes et al., 2017), however, indicated that other environmental variables (as topography and weather) had a higher influence on burn severity than fuel characteristics. Another variable related in our study to pre-fire vegetation was TCD. According to RF variable importance analysis, it had a low relevance when using the input database 1, being even lower when ET variable was included (databases 2 and 3). Turner et al. (1999) have also found that the relationship between burn severity and pre-fire tree density was not significant. By contrast,

Table 3
Summary of accuracy parameters.

Accuracy parameters								
	Input database 1		Input database 2		Input database 3		Input database 4	
κ statistic	0.72		0.71		0.79		0.76	
σκ	0.0003		0.0003		0.0002		0.0002	
Margin of Error (CI)	0.0319		0.0326		0.0304		0.0308	
Lower Bound	0.68		0.67		0.76		0.72	
Upper Bound	0.75		0.74		0.83		0.78	
PA	0.75		0.73		0.81		0.80	
UA	0.77		0.75		0.82		0.79	
OA	0.80		0.80		0.86		0.83	
	PA_{class}	UA_{class}	PA_{class}	UA_{class}	PA_{class}	UA_{class}	PA_{class}	UA_{class}
Unburned	0.85	0.91	0.89	0.92	0.90	0.94	0.87	0.93
Low	0.61	0.45	0.54	0.36	0.65	0.54	0.63	0.59
Moderate	0.72	0.76	0.71	0.80	0.81	0.82	0.77	0.79
High	0.87	0.88	0.87	0.84	0.92	0.93	0.91	0.87

Z-test				
	Input database 1	Input database 2	Input database 3	Input database 4
Input database 1		0.43	3.89	1.98
Input database 2	0.43		4.13	2.32
Input database 3	3.89	4.13		1.99
Input database 4	1.98	2.32	1.99	

Input data base 1: char_sn, fuel model, TCD, climate, elevation, slope and aspect; input data base 2: ET, fuel model, TCD, climate, elevation, slope and aspect; input data base 3: char_sn, ET, fuel model, TCD, climate, elevation, slope and aspect; input data base 4: char_sn, ET; PA: producer's accuracy; UA: user's accuracy; OA: overall accuracy.

Birch et al. (2015) found the percentage of vegetation cover as a relevant factor of burn severity. TCD had a low variability in our study area as all forested areas showed a high cover density. That is likely the reason for its low influence. It is presumed that in areas with higher TCD variability, this variable may exert a potentially higher influence on burn severity.

Climate was ranked by RF as the fourth most important variable in our study. Köppen climatic classes included information on average precipitation level and mean temperature range that have important impact on vegetation characteristics. Pre-fire precipitation and temperature have an established strong influence on fire severity, especially under extreme conditions (Bigler et al., 2005; Nunes et al., 2005). However, under more moderate climatic conditions, the influence of climate was lower than the influence of topography and fuels (Bradstock et al., 2010).

Topographic variables also had a relevant contribution to burn severity in our study. RF ranked elevation as the second most important variable when used in database 1 (although its importance was very similar to fuel model and climate). Aspect was the second important variable when database 2 was used (it was very close in importance to fuel model), but elevation and slope were also relevant contributors to burn severity. When using input database 3, aspect and elevation had moderate importance on burn severity as well (fifth and sixth positions). Many studies (e.g. Estes et al., 2017; Lee et al., 2009; Mitsopoulos et al., 2019; Viedma et al., 2014) have pointed out the strong influence of topography on burn severity. Wind patterns and microclimate are influenced by topographic attributes (Mitsopoulos et al., 2019). In particular, slope and aspect have an effect on fuel moisture, which directly influences fire intensity (Rothermel, 1972) and on fuel composition and availability (Holden et al., 2009). Level of topographic complexity of terrain may define, however, the level of influence of topography on burn severity (Estes et al., 2017). A complex topography exerts a strong influence on burn severity (Bradstock et al., 2010; Oliveras et al., 2009; Wimberly and Reilly, 2007). Whereas little relationship between burn severity and topography has been found in regions with low variability in topographic attributes (Collins et al., 2007; Turner et al., 1999). The moderate association between topographic characteristics and burn severity found in our study area is in correspondence with its moderate level of topographical complexity.

Although low and moderate burn severity levels had lower PA and UA values than high burn severity and unburned classes, the RF classifier accurately mapped burn severity using three burn severity levels (κ = 0.79). This agrees with Collins et al. (2018) who highlighted the capability of RF to discriminate low and moderate burn severity levels, enabling an accurate burn severity estimate with three levels of severity. In the same study area, Brown et al. (2018) estimated three burn severity from Sentinel spectral indices using Artificial Neural Networks (ANN's) (κ = 0.66) and Support Vector Machines (SVMs) (κ = 0.71). They also observed lower PA and UA accuracy in low and moderate classes. RF has already been successfully used to estimate burn severity in previous studies: Collins et al. (2018) reached accuracy values higher than 95% for unburned, and high burn severity classes and higher than 74% for low burn severity classes using a RF trained with multiple Landsat-derived pre- and post-fire spectral indices in sixteen fires located in south-eastern Australia. Parks et al. (2019) implemented RF in Google Earth Engine and modeled CBI in 263 fires both in USA and Canada, reaching a R^2 of 0.72. As inputs they used spectral indices, climatic and geographic data. Meng et al. (2017) used as RF inputs modified soil-adjusted vegetation index difference (dMSAVI) and MESMA fraction images. Their aim was to estimate burn severity with three levels in a Pine Barrens region in Long Island (USA). They obtained a κ statistic value of 0.77 at sub-crown level and of 0.76 at crown level.

Regarding our initial research questions, we can affirm that it is possible to obtain an accurate burn severity estimate from fine-resolution post-fire ET, in particular, with similar accuracy to MESMA char fraction based one (e.g. Meng et al., 2017; Quintano et al.,

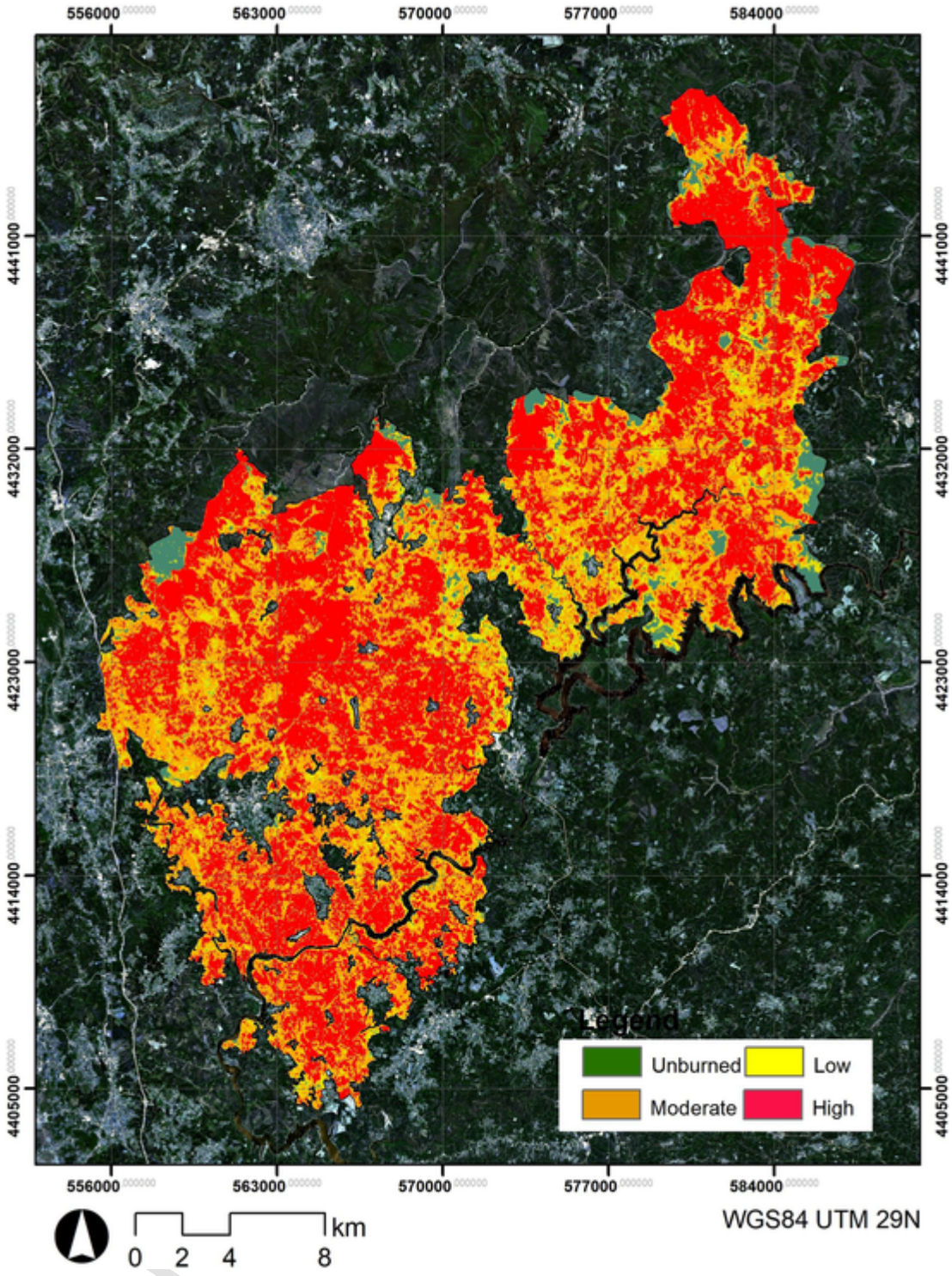

Fig. 6. Burn severity map based on RF classification of input database 3: (char_sn, ET, fuel model, TCD, climate, elevation, slope and aspect).

2019; Tane et al., 2018) (question 1). The combination of ET and MESMA char fraction image enabled a burn severity estimate with higher accuracy. We found a synergetic interaction between these two variables when both were used to modeling burn severity with the RF classifier (question 2). Moreover, the physical meaning of both MESMA char fraction and fine resolution ET facilitated the understanding of their relationships to burn severity, especially when it was compared to the difficult to interpret relationship among burn severity and spectral indices (Morgan et al., 2014). Adding environmental variables, particularly fuel model, climate class, elevation and aspect, as inputs to the RF classifier increased the accuracy of burn severity estimate ($\kappa = 0.79$) (question 3). Our research work proposed a novel and promising procedure that should be validated in more fire events. However, although we studied only one fire, it was one of the most important wildfires in size and damage (vegetation, buildings and people) happened in European Mediterranean countries (San-Miguel-Ayanz et al., 2018). In addition, our study area was located in the transition zone of two Mediterranean Köppen

climactic classes (Csa and Csb), Future research should test this methodology in other Mediterranean ecosystems around the world. Moreover, in spite of the fact that our study area corresponded to a Mediterranean ecosystem, we believe the proposed methodology could be applied successfully in other ecosystems as well.

6. Conclusions

Fire has a great impact on ET, affecting water balance as well. Our study verified the usefulness of Landsat-derived post-fire ET to estimate burn severity in Mediterranean ecosystems using a RF classifier. The accuracy of the ET-based estimate was similar to the accuracy of the estimate based on MESMA Sentinel-2 char fraction ($\kappa = 0.71$ and $\kappa = 0.72$ respectively). MESMA compressed all spectral information contained in a post-fire Sentinel-2 image into three fraction images with physical meaning. The accurate burn severity estimation based on char fraction image would not have been possible without an organized and careful building of the spectral library used to unmix the Sentinel-2 image. Spectra of all land covers present in the study area were included in the library and grouped as char, GV and NPVSW. Moreover, we observed that the combined use of fine-resolution ET and MESMA char fraction as RF inputs increased the accuracy of burn severity estimate ($\kappa = 0.76$ and $\kappa = 0.79$, if pre-fire vegetation, climate and topographic variables were included as well as RF inputs). In these cases, char fraction image would incorporate the fire-induced change on spectral information, and ET would contribute with information on water balance alterations due to fire. A clear advantage of these two input variables versus the commonly used spectral indices is their easier interpretation in relation to burn severity as both of them have a clear physical meaning. Additionally, the use of RF as classifier allowed us to evaluate the contribution of each input variable to the modeling process of burn severity. ET was the variable with the highest contribution, followed by MESMA char faction image. Fuel model, climate and topographic variables also had a noticeable contribution, although lower than ET and char fraction image. Summarizing, our study proved the potential use of fine resolution ET to estimate burn severity, especially when it was used together to MESMA char fraction, as synergetic interactions between these two variables were observed for modeling burn severity. The novel proposed methodology enables analyzing fire impact on vegetation, which in turn may help to improve post-fire management policies. Though the study was located in Mediterranean ecosystem, the proposed method may be generalized to fires happened in other ecosystems. In addition, it might take advantage of the new ECOSTREES mission that will provide fine-resolution ET images worldwide.

CRediT authorship contribution statement

Carmen Quintano: Conceptualization, Methodology, Software, Formal analysis, Validation, Writing - original draft, Writing - review & editing.**Alfonso Fernandez-Manso:**Conceptualization, Methodology, Software, Formal analysis, Validation, Writing - original draft, Writing - review & editing.**Dar A. Roberts:**Conceptualization, Supervision, Writing - review & editing.

Declaration of competing interest

The authors declare that they have no known competing financial interests or personal relationships that could have appeared to influence the work reported in this paper.

Acknowledgments

This research was funded by the Spanish Ministry of Economy and Competitiveness (FIRESEVES project, 559 AGL2017-86075-C2-1-R), and the Regional Government of Castile and León (SEFIRECYL project, LE001P17). The two first authors were supported as research visitors at VIPER Lab. (University of California, Santa Barbara) by Spanish Education Ministry grants (Salvador de Madariaga program, codes PRX19/00021 and PRX19/00052).

References

ADAI/LAETA, 2017. O complexo de incêndios de Pedrógão grande e concelhos limítrofes, iniciado a 17 de junho de 2017. Universidade de Coimbra Official report. República portuguesa (in portuguese).

Addinsoft XLSTAT Version 19.3.2https://www.xlstat.com2019

Agee, J K, Skinner, C N, 2005. Basic principles of forest fuel reduction treatments. Forest Ecol. Manag. 211, 83–96. doi:10.1016/j.foreco.2005.01.034.

Ahmed, O S, Franklin, S E, Wulder, M A, White, J C, 2015. Characterizing stand-level forest canopy cover and height using Landsat time series, samples of airborne LiDAR, and the Random Forest algorithm. ISPRS J. Photogramm. Remote Sens. 101, 89–101. doi:10.1016/j.isprsjprs.2014.11.007.

Alkama, R, Cescatti, A, 2016. Biophysical climate impacts of recent changes in global forest cover. Science 351 (6273), 600–604. doi:10.1126/science.aac8083.

Allen, R G, Tasumi, M, Trezza, R, 2007. Satellite-based energy balance for mapping evapotranspiration with internalized calibration (METRIC)-model. J. Irrig. Drain. Eng. 133, 380–394.

Allen, R, Morton, C, Kamble, B, Kilic, A, Huntington, J, Thau, D, Gorelick, N, Erickson, T, Moore, R, Trezza, R, Ratcliffe, I, Robison, C, 2015. EEFlux: A Landsat-based Evapotranspiration mapping tool on the Google Earth Engine. 2015 ASABE Irrigation Symposium. Paper Number: 152143511. In: Technologies for Sustainable Irrigation Proceedings of the 10–12 November 2015 Symposium, Long Beach, California USA. Published by ASABE (Publication No. 701P0415).

Amos, C, Petropoulos, G P, Ferentinos, K P, 2019. Determining the use of Sentinel-2A MSI for wildfire burning & severity detection. Int. J. Remote Sens. 40, 905–930.

Anderson, H, 1982. Aids to Determining Fuel Models for Estimating Fire Behavior, USDA Forest Service, Ogden, Utah: Report INT-122.

Atchley, A L, Kinoshita, A M, Lopez, S R, Trader, L, Middleton, R, 2018. Simulating surface and subsurface water balance changes due to burn severity. Vadose Zone J. 17, 180099. doi:10.2136/vzj2018.05.0099.

Baldocchi, D, Falge, E, Gu, L, Olson, R, Hollinger, D, Running, S, Anthoni, P, Bernhofer, C H, Davis, K, Evans, R, Fuentes, J, Goldstein, A, Katul, G, Law, B, Lee, X, Malhi, Y, Meyers, T, Munger, W, Oechel, W, U., K T P, Pilegaard, K, Schmid, H P, Valentini, R, Verma, S, Vesala, T, Wilson, K, Wofsy, S, 2001. FLUXNET: a new tool to study the temporal and spatial variability of ecosystem-scale carbon dioxide, water vapor, and energy flux densities. Bull. Am. Meteorol. Soc. 82 (11), 2415–2434.

Belgiu, M, Drăguţ, L, 2016. Random forest in remote sensing: a review of applications and future directions. ISPRS J. Photogramm. Remote Sens. 114, 24–31.

Bigler, C, Kulakowski, D, Veblen, T T, 2005. Multiple disturbance interactions and drought influence fire severity in Rocky Mountain subalpine forests. Ecology 86, 3018–3029.

Birch, D S, Morgan, P, Kolden, C A, Abatzoglou, J T, Dillon, G K, Hudak, A T, Smith, A M S, 2015. Vegetation, topography and daily weather influenced burn severity in central Idaho and western Montana forests. Ecosphere 6, art17. doi:10.1890/es14-00213.1.

Bradstock, R A, Hammill, K A, Collins, L, Price, O, 2010. Effects of weather, fuel and terrain on fire severity in topographically diverse landscapes of south-eastern Australia. Landsc. Ecol. 25, 607–619.

Breiman, L, 1996. Bagging predictors. Mach. Learn. 24, 123–140.

Breiman, L, 2001. Random forests. Mach. Learn. 45, 5–32.

Brown, A R, Petropoulos, G P, Ferentinos, K P, 2018. Appraisal of the Sentinel-1 & 2 use in a large-scale wildfire assessment: a case study from Portugal's fires of 2017. Appl. Geogr. 100, 78–89. doi:10.1016/j.apgeog.2018.10.004.

Cai, X, Riley, W J, Zhu, Q, Tang, J, Zeng, Z, Bisht, G, Randerson, J T, 2019. Improving representation of deforestation effects on evapotranspiration in the E3SM land model. J. Adv. Model. Earth Sy. 11 (8), 2412–2427. doi:10.1029/2018ms001551.

Calvo, L, Santalla, S, Valbuena, L, Marcos, E, Tárrega, R, Luis-Calabuig, E, 2008. Postfire natural regeneration of a Pinus pinaster forest in NW Spain. Plant Ecol. 197, 81–90. doi:10.1007/s11258-007-9362-1.

Camargo, F F, Sano, E E, Almeida, C M, Mura, J C, Almeida, T, 2019. A comparative assessment of machine-learning techniques for land use and land cover classification of the Brazilian tropical savanna using ALOS-2/PALSAR-2 polarimetric images. Remote Sens. 11, 1600. doi:10.3390/rs11131600.

Chrysafis, I, Mallinis, G, Gitas, I, Tsakiri-Strati, M, 2017. Estimating Mediterranean forest parameters using multi seasonal Landsat 8 OLI imagery and an ensemble learning method. Remote Sens. Environ. 199, 154–166.

Clark, K L, Skowronski, N, Gallagher, M, Renninger, H, Schäfer, K, 2012. Effects of invasive insects and fire on forest energy exchange and evapotranspiration in the New Jersey pinelands. For. Meteorol. 166, 50–61.

Collins, B M, Kelly, M, van Wagtendonk, J W, Stephens, S L, 2007. Spatial patterns of large natural fires in Sierra Nevada wilderness areas. Landsc. Ecol. 22, 545–557.

Collins, L, Griffioen, P, Newell, G, Mellor, A, 2018. The utility of Random Forests for wildfire severity mapping. Remote Sens. Environ. 216, 374–384.

Congalton, R G, Green, K, 2009. Assessing the Accuracy of Remotely Sensed Data. Principles and Practices. 2 edition CRC Press. Taylor & Francis, Boca Ratón.

CTI, 2017. Análise e apuramento dos factos relativos aos incêndios que ocorreram em Pedrógão Grande, Castanheira de Pêra, Ansião, Alvaiázere, Figueiró dos Vinhos, Arganil, Góis, Penela, Pampilhosa da Serra, Oleiros e Sertã entre 17 e 24 de junho de 2017. Assembleia da República.

Cutler, D R, Edwards, T C, Beard, K H, Cutler, A, Hess, K T, Gibson, J, Lawler, J J, 2007. Random forests for classification in ecology. Ecology 88, 2783–2792. doi:10.1890/07-0539.1.

de la Fuente-Sáiz, D, Ortega-Farí, S, Fonseca, D, Ortega-Salazar, S, Kilic, A, Allen, R, 2017. Calibration of METRIC model to estimate energy balance over a drip-irrigated apple orchard. Remote Sens. 9, 670. doi:10.3390/rs9070670.

Dennison, P E, Roberts, D A, 2003. Endmember selection for mapping chaparral species and fraction using Multiple Endmember Spectral Mixture Analysis. Remote Sens. Environ. 41, 123–135.

Dennison, P E, Halligan, K Q, Roberts, D A, 2004. A comparison of error metrics and constraints for Multiple Endmember Spectral Mixture Analysis and Spectral Angle Mapper. Remote Sens. Environ. 93, 359–367.

Dennison, P E, Qi, Y, Meerdink, S K, Kokaly, R F, Thompson, D R, Daughtry, C S T, Quemada, M, Roberts, D A, Gader, P D, Wetherley, E B, Numata, I, Roth, K L, 2019. Comparison of methods for modeling fractional cover using simulated satellite hyperspectral imager spectra. Remote Sens. 11, 2072. doi:10.3390/rs11182072.

DGT, 2018. Especificações técnicas da Carta de uso e ocupação do solo de Portugal Continental para 1995, 2007, 2010 e 2015. Relatório Técnico. Direção-Geral do Território.

Dillon, G K, Holden, Z A, Morgan, P, Crimmins, M A, Heyerdahl, E K, Luce, C H, 2011. Both topography and climate affected forest and woodland burn severity in two regions of the western US, 1984 to 2006. Ecosphere 2 (12), 130. doi:10.1890/ES11-00271.1.

Dore, S, Kolb, T E, Montes-Helu, M, Eckert, S E, Sullivan, B W, Hungate, B A, Kaye, J P, Hart, S C, Koch, G W, Finkral, A, 2010. Carbon and water fluxes from ponderosa pine forests disturbed by wildfire and thinning. Ecol. Appl. 20, 663–683.

Dudley, K L, Dennison, P E, Roth, K L, Roberts, D A, Coates, A R, 2015. A multi-temporal spectral library approach for mapping vegetation species across spatial and temporal phenological gradients. Remote Sens. Environ. 167, 121–134.

Ellison, D, Morris, C E, Locatelli, B, Sheil, D, Cohen, J, Murdiyarso, D, Gutierrez, V, van Noordwijkl, M, Creed, I F, Pokorny, J, Gaveau, D, Spracklen, D V, Tobella, A B, Ilstedt, U, Teuling, A J, Gebrehiwot, S G, Sands, D C, Muys, B, Verbist, B, Springgay, E, Sugandiv, Y, Sullivan, C A, 2017. Trees, forests and water: cool insights for a hot world. Global Environ. Chang. 43, 51–61. doi:10.1016/j.gloenvcha.2017.01.002.

Epting, J, Verbyla, D, Sorbel, B, 2005. Evaluation of remotely sensed indices for assessing burn severity in interior Alaska using Landsat TM and ETM+. Remote Sens. Environ. 96, 328–339.

ESA, 2015. Sentinel-2 User Handbook. ESA, Paris, France Available online. https://earth.esa.int/web/sentinel/user-guides/sentinel-2-msi (accessed on 26 September 2019).

Estes, B L, Knapp, E E, Skinner, C N, Miller, J D, Preisler, H K, 2017. Factors influencing fire severity under moderate burning conditions in the Klamath Mountains, northern California USA. Ecosphere 8, e01794. doi:10.1002/ecs2.1794.

Fang, L, Yang, J, White, M, Liu, Z, 2018. Predicting potential fire severity using vegetation, topography and surface moisture availability in a Eurasian boreal forest landscape. Forests 9 (3), 130. doi:10.3390/f9030130.

Fernandes, P, Gonçalves, H, Loureiro, C, Fernandes, M, Costa, T, Cruz, M G, Botelho, H, 2009. Modelos de combustível florestal para Portugal. In: Proceedings of 6° Congresso Florestal Nacional. SPCF, Lisboa, pp. 348–354.

Fernández-Manso, O, Quintano, C, Fernández-Manso, A, 2009. Combining spectral mixture analysis and object-based classification for fire severity mapping. Forest Sys 18, 296–313.

Fernández-Manso, A, Quintano, C, Roberts, D A, 2012. Evaluation of potential of multiple endmember spectral mixture analysis (MESMA) for surface coal mining affected area mapping in different world forest ecosystems. Remote Sens. Environ. 127, 181–193.

Fernández-Manso, O, Quintano, C, Fernández-Manso, A, 2016. SENTINEL-2A red-edge spectral indices suitability for discriminating burn severity. Int. J. Appl. Earth Obs. 50, 170–175.

Fernández-Manso, A, Quintano, C, Roberts, D A, 2016. Burn severity influence on postfire vegetation cover resilience from Landsat MESMA fraction images time series in Mediterranean forest ecosystems. Remote Sens. Environ. 184, 112–123.

Fernández-Manso, A, Quintano, C, Roberts, D A, 2019. Burn severity analysis in Mediterranean forests using maximum entropy model trained with EO-1 Hyperion and LiDAR data. ISPRS J. Photogramm. Remote Sens. 155, 102–118.

Finney, M A, McHugh, C, Grenfell, I C, 2005. Stand- and landscape-level effects of prescribed burning on two Arizona wildfires. Can. J. For. Res. 35, 1714–1722.

Fisher, J B, Hook, R, Allen, R G, Anderson, M C, French, A N, Hain, C R, Hulley, G, Wood, E F, 2014. The ECOsystem Spaceborne Thermal Radiometer Experiment on Space Station (ECOSTRESS): science motivation. In: American Geophysical Union Fall Meeting. San Francisco, USA. Abstract id. H31J-07.

Fisher, J B, Melton, F, Middleton, E, Hain, C, Anderson, M, Allen, R, McCabe, M F, Hook, S, Baldocchi, D, Townsend, P A, Kilic, A, Tu, K, Miralles, D D, Perret, J, Lagouarde, J-P, Waliser, D, Purdy, A J, French, A, Schimel, D, Famiglietti, J S, Stephens, G, Wood, E F, 2017. The future of evapotranspiration: global requirements for ecosystem functioning, carbon and climate feedbacks, agricultural management, and water resources. Water Resour. Res. 53, 2618–2626. doi:10.1002/2016WR020175.

García-Llamas, P, Suárez-Seoane, S, Fernández-Guisuragaa, J M, Fernández-García, V, Fernández-Manso, A, Quintano, C, Taboada, A, Marcos, E, Calvo, L, 2019. Evaluation and comparison of Landsat 8, Sentinel-2 and Deimos-1 remote sensing indices for assessing burn severity in Mediterranean fire-prone ecosystems. Int. J. Appl. Earth Obs. 80, 137–144.

García-Llamas, P, Suárez-Seoane, S, Taboada, A, Fernández-García, V, Fernández-Guisuraga, J M, Fernández-Manso, A, Quintano, C, Marcos, E, Calvo, L, 2019. Assessment of the influence of biophysical properties related to fuel conditions on fire severity using remote sensing techniques: a case study on a large fire inNW Spain. Int. J. Wildland Fire 28, 512–520. doi:10.1071/WF18156.

Gislason, P O, Benediktsson, J A, Sveinsson, J R, 2006. Random Forests for land cover classification. Pattern Recogn. Lett. 27, 294–300. doi:10.1016/j.patrec.2005.08.011.

González-de Vega, S, de las Heras, J, Moya, D, 2018. Post-fire regeneration and diversity response to burn severity in Pinus halepensis Mill. Forest. Forest 9, 299. doi:10.3390/F9060299.

Harris, L, Taylor, A H, 2017. Previous burns and topography limit and reinforce fire severity in a large wildfire. Ecosphere 8, e02019. doi:10.1002/ECS2.2019.

Hastie, T J, Tibshirani, R J, Friedman, J H, 2009. The Elements of Statistical Learning: Data Mining, Inference, and Prediction. Springer, New York, NY, USA.

Häusler, M, Nunes, J P, Soares, P, Sánchez, J M, Silva, J M N, Warneke, T, Keizer, J J, Pereira, J M C, 2018. Assessment of the indirect impact of wildfire (severity) on actual evapotranspiration in eucalyptus forest based on the surface energy balance estimated from remote-sensing techniques. Int. J. Remote Sens. 39, 6499–6524. doi:10.1080/01431161.2018.1460508.

He, Y, Chen, G, de Santis, A, Roberts, D A, Zhou, Y, Meentemeyer, R K, 2019. A disturbance weighting analysis model (DWAM) for mapping wildfire burn severity in the presence of forest disease. Remote Sens. Environ. 221, 108–121. doi:10.1016/j.rse.2018.11.015.

Holden, Z A, Morgan, P, Evans, J S, 2009. A predictive model of burn severity based on 20-year satellite-inferred burn severity data in a large southwestern US wilderness area. Forest Ecol. Manag. 258, 2399–2406.

Hudak, A, Morgan, P, Bobbitt, M, Smith, A, Lewis, S, Lentile, L, Robichaud, P, Clark, J, McKinley, R, 2007. The relationship of multispectral satellite imagery to immediate fire effects. Fire Ecol 3, 64–90.

Hudak, A T, Crookston, N L, Evans, J S, Hall, D E, Falkowski, M J, 2008. Nearest neighbor imputation of species-level, plot-scale forest structure attributes from LiDAR data. Remote Sens. Environ. 112, 2232–2245.

Hultquist, C, Chen, G, Zhao, K, 2014. A comparison of Gaussian process regression, random forests and support vector regression for burn severity assessment in diseased forests. Remote Sens. Lett. 5, 723–732.

Irmak, A, Allen, R G, Kjaersgaard, J, Huntington, J, Kamble, B, Trezza, R, Ratcliffe, I, 2011. Operational Remote Sensing of ET and Challenges. In Evapotranspiration – Remote Sensing and Modeling. Ayse Irmak (526 pp. ISBN 978-953-307-808-3).

Jain, T B, Pilliod, D, Graham, R T, 2004. Tongue-tied. Confused meanings for common fire terminology can lead to fuels mismanagement. A new framework is needed to clarify and communicate the concepts. Wildfire 4, 22–26.

Kane, V R, Lutz, J A, Cansler, C A, Povak, N A, Churchill, D J, Smith, D F, Kane, J T, North, P M, 2015. Water balance and topography predict fire and forest structure patterns. For. Ecol. Manag. 338, 1–13. doi:10.1016/j.rse.2013.07.041.

Key, C H, Benson, N C, 2006. Landscape assessment: ground measure of severity, the composite burn index; and remote sensing of severity, the normalized burn ratio. In: Lutes, D C, Keane, R E, Caratti, J F, Key, C H, Benson, N C, Sutherland, S, Gangi, L J (Eds.), FIREMON: Fire Effects Monitoring and Inventory System. USDA Forest Service, Rocky Mountain Research Station, Ogden, UT. Gen. Tech. Rep. RMRSGTR-164-CD, LA, pp. 1–51.

Köppen, W, 1936. Das geographische System der Klimate. 1936. Gebrüder Borntraeger, Berlin, Germany, pp. 1–44.

Kraaij, T, Baard, J A, Arndt, J, Vhengani, L, van Wilgen, B W, 2018. An assessment of climate, weather, and fuel factors influencing a large, destructive wildfire in the Knysna region, South Africa. Fire Ecol 14, 4. doi:10.1186/s42408-018-0001-0.

Kuenzi, A M, Fulé, P Z, Sieg, C H, 2008. Effects of fire severity and pre-fire stand treatment on plant community recovery after a large wildfire. For. Ecol. Manag. 255, 855–865. doi:10.1016/j.foreco.2007.10.001.

Lawrence, R L, Wood, S D, Sheley, R L, 2006. Mapping invasive plants using hyperspectral imagery and Breiman Cutler classifications (randomForest). Remote Sens. Environ. 100, 356–362.

Lee, S-W, Lee, M-B, Lee, Y-G, Won, M-S, Kim, J-J, Hong, S-K, 2009. Relationship between landscape structure and burn severity at the landscape and class levels in Samcheock, South Korea. For. Ecol. Manag. 258, 1594–1604.

Lentile, L, Holden, Z, Smith, A, Falkowski, M, Hudak, A, Morgan, P, Lewis, S, Gessler, P, Benson, N, 2006. Remote sensing techniques to assess active fire characteristics and post-fire effects. Int. J. Wildland Fire 15, 319–345.

Lentile, L, Smith, A, Hudak, A, Morgan, P, Bobbitt, M, Lewis, S, Robichaud, P, 2009. Remote sensing for prediction of 1-year post-fire ecosystem condition. Int. J. Wildland Fire 18, 594–608.

Lewis, S A, Robichaud, P R, Hudak, A T, Austin, B, Liebermann, R J, 2012. Utility of remotely sensed imagery for assessing the impact of salvage logging after forest fires. Remote Sens. 4, 2112–2132. doi:10.3390/rs4072112.

Lewis, S A, Hudak, A T, Robichaud, P R, Morgan, P, Satterberg, K L, Strand, E K, Smith, A M S, Zamudio, J A, Lentile, L B, 2017. Indicators of burn severity at extended temporal scales: a decade of ecosystem response in mixed-conifer forests of western Montana. Int. J. Wildland Fire 26, 755–771. doi:10.1071/WF17019.

Li, Y, Piao, S, Li, L Z X, Chen, A, Wang, X, Ciais, P, Huang, L, Lian, X, Peng, S, Zeng, Z, Wang, K, Zhou, L, 2018. Divergent hydrological response to large-scale afforestation and vegetation greening in China. Sci. Adv. 4 (5). doi:10.1126/sciadv.aar4182.

Li, X, Zhang, H, Yang, G, Ding, Y, Zhao, J, 2018. Post-fire vegetation succession and surface energy fluxes derived from remote sensing. Remote Sens. 10, 1000. doi:10.3390/rs10071000.

Liaw, A, Wiener, M, 2002. Classification and regression by random Forest. R News 2 (3), 18–22.
Lydersen, J M, Collins, B M, Brooks, M L, Matchett, J R, Shive, K L, Povak, N A, Kane, V R, Smith, D F, 2017. Evidence of fuels management and fire weather influencing fire severity in an extreme fire event. Ecol. Appl. 27, 2013–2030. doi:10.1002/EAP.1586.
Mahdianpari, M, Salehi, B, Mohammadimanesh, F, Motagh, M, 2017. Random forest wetland classification using ALOS-2 L-band, RADARSAT-2 C-band, and TerraSAR-X imagery. ISPRS J. Photogramm. Remote Sens. 130, 13–31. doi:10.1016/j.isprsjprs.2017.05.010.
Mallinis, G, Mitsopoulos, I, Chrysafi, I, 2017. Evaluating and comparing Sentinel 2A and Landsat-8 Operational Land Imager (OLI) spectral indices for estimating fire severity in a Mediterranean pine ecosystem of Greece. GISci. Remote Sens. 55, 1–18.
Mather, P, Tso, B, 2016. Classification Methods for Remotely Sensed Data. CRC press.
Meddens, A J H, Kolden, C A, Lutz, J A, 2016. Detecting unburned areas within wildfire perimeters using Landsat and ancillary data across the northwestern United States. Remote Sens. Environ. 186, 275–285.
Mellor, A, Boukir, S, Haywood, A, Jones, S, 2015. Exploring issues of training data imbalance and mislabelling on Random Forest performance for large area land cover classification using the ensemble margin. ISPRS J. Photogramm. Remote Sens. 105, 155–168. doi:10.1016/j.isprsjprs.2015.03.014.
Meng, R, Wu, J, Schwager, K L, Zhao, F, Dennison, P E, Cook, B D, Brewster, K, Green, T M, Serbin, S P, 2017. Using high spatial resolution satellite imagery to map forest burn severity across spatial scales in a Pine Barrens ecosystem. Remote Sens. Environ. 2017 (191), 95–109. doi:10.1016/j.rse.2017.01.016.
Miller, J D, Thode, A E, 2007. Quantifying burn severity in a heterogeneous landscape with a relative version of the delta normalized burn ratio (dNBR). Remote Sens. Environ. 109, 66–80.
Miller, J D, Knapp, E E, Key, C H, Skinner, C N, Isbell, C J, Creasy, R M, Sherlock, J W, 2009. Calibration and validation of the relative differenced normalized burn ratio (RdNBR) to three measures of fire severity in the Sierra Nevada and Klamath Mountains, California, USA. Remote Sens. Environ. 113, 645–656.
Mitsopoulos, I, Chrysafi, I, Bountis, D, Mallinis, G, 2019. Assessment of factors driving high fire severity potential and classification in a Mediterranean pine ecosystem. J. Environ. Manag. 235, 266–275.
Montes-Helu, M C, Kolb, T, Dore, S, Sullivan, B, Hart, S C, Koch, G, Hungate, B A, 2009. Persistent effects of fire-induced vegetation change on energy partitioning and evapotranspiration in ponderosa pine forests. Agric. For. Meteorol. 149, 491–500.
Morgan, P, Keane, R E, Dillon, G K, Jain, T B, Hudak, A T, Karau, E C, Sikkink, P G, Holden, Z A, Strand, E K, 2014. Challenges of assessing fire and burn severity using field measures, remote sensing and modeling. Int. J. Wildland Fire 23, 1045–1060.
Naidoo, L, Cho, M A, Mathieu, R, Asner, G, 2012. Classification of savanna tree species, in the Greater Kruger National Park region, by integrating hyperspectral and LiDAR data in a Random Forest data mining environment. ISPRS J. Photogramm. Remote Sens. 69, 167–179. doi:10.1016/j.isprsjprs.2012.03.005.
Nolan, R H, Lane, P N J, Benyon, R G, Bradstock, R A, Mitchell, P J, 2014. Changes in evapotranspiration following wildfire in resprouting eucalypt forests. Ecohydrology 7, 1363–1377.
Nunes, M C S, Vasconcelos, M J, Pereira, J M C, Dasgupta, N, Alldredge, R J, Rego, F C, 2005. Land cover type and fire in Portugal: do fires burn land cover selectively? Landsc. Ecol. 20, 661–673.
Oliveras, I, Gracia, M, More, G, Retana, J, 2009. Factors influencing the pattern of fire severities in a large wildfire under extreme meteorological conditions in the Mediterranean basin. Int. J. Wildland Fire 18, 755–764.
Parks, S A, Holsinger, L M, Koontz, M J, Collins, L, Whitman, E, Parisien, M-A, Loehman, R A, Barnes, J L, Bourdon, J-F, Boucher, J, Boucher, Y, Caprio, A C, Collingwood, A, Hall, R J, Park, J, Saperstein, L B, Smetanka, C, Smith, R J, Soverel, N, 2019. Giving ecological meaning to satellite-derived fire severity metrics across North American forests. Remote Sens. 11, 1735. doi:10.3390/rs11141735.
Pausas, J G, Llovet, J, Rodrigo, A, Vallejo, R, 2008. Are wildfires a disaster in the Mediterranean basin? – a review. Int. J. Wildfire Fire 17, 713–723. doi:10.1071/WF07151.
Pedregosa, F, Varoquaux, G, Gramfort, A, Michel, V, Thirion, B, Grisel, O, Blondel, M, Prettenhofer, P, Weiss, R, Dubourg, V, Vanderplas, J, Passos, A, Cournapeau, D, Brucher, M, Perrot, M, Duchesnay, E, 2011. Scikit-learn: machine learning in python. J. Mach. Learn. Res. 12, 2825–2830.
Peel, M C, Finlayson, B L, McMahon, T A, 2007. Updated world map of the Köppen-Geiger climate classification. Hydrol. Earth Syst. Sci. 11, 1633–1644. doi:10.5194/hess-11-1633-2007.
Pérez-Cabello, F, Echeverría, M T, Ibarra, P, de la Riva, J, 2009. Effects of fire on vegetation, soil and hydrogeomorphological behavior in Mediterranean ecosystems. In: Chuvieco, E (Ed.), Earth Observation of Wildland Fires in Mediterranean Ecosystems. Springer, Berlin, Germany, pp. 111–128.
Poon, P K, Kinoshita, A M, 2018. Spatial and temporal evapotranspiration trends after wildfire in semi-arid landscapes. J. Hydrol. 559, 71–83. doi:10.1016/j.jhydrol.2018.02.023.
Quintano, C, Fernández-Manso, A, Fernández-Manso, O, Shimabukuro, Y E, 2006. Mapping burned areas in Mediterranean countries using spectral mixture analysis from a uni-temporal perspective. Int. J. Remote Sens. 27, 645–662. doi:10.1080/01431160500212195.
Quintano, C, Fernández-Manso, A, Shimabukuro, Y E, Pereira, G, 2012. Spectral unmixing. Int. J. Remote Sens. 33, 5307–5340.
Quintano, C, Fernández-Manso, A, Roberts, D A, 2013. Multiple Endmember Spectral Mixture Analysis (MESMA) to map burn severity levels from Landsat images in Mediterranean countries. Remote Sens. Environ. 136, 76–88.
Quintano, C, Fernández-Manso, A, Roberts, D A, 2017. Burn severity mapping from Landsat MESMA fraction images and land surface temperatures. Remote Sens. Environ. 190, 83–95.
Quintano, C, Fernández-Manso, A, Calvo, L, Roberts, D A, 2019. Vegetation and soil fire damage analysis based on species distribution modeling trained with multispectral satellite data. Remote Sens. 11, 1832. doi:10.3390/rs11151832.
Ramo, R, Chuvieco, E, 2017. Developing a random forest algorithm for MODIS global burned area classification. Remote Sens. 9, 1193.
Randerson, J T, Liu, H, Flanner, M G, Chambers, S D, Jin, Y, Hess, P G, Pfister, G, Mack, M C, Treseder, K K, Welp, L R, Chapin, F S, Harden, J W, Goulden, M L, Lyons, E, Neff, J C, Schuur, E A G, Zender, C S, 2006. The impact of boreal forest fire on climate warming. Science 314, 1130–1132.
Ribeiro, L M, Rodrigues, A, Lucas, D, Viegas, D X, 2018. The large fire of Pedrógão Grande (Portugal) and its impact on structures. In: Viegas, D X (Ed.), Advances in Forest Fire Research 2018. pp. 852–858. doi:10.14195/978-989-26-16-506_94.
Roberts, D A, Smith, M O, Adams, J B, 1993. Green vegetation, non-photosynthetic vegetation, and soils in AVIRIS data. Remote Sens. Environ. 44, 255–269.
Roberts, D A, Gardner, M, Church, R, Ustin, S, Scheer, G, Green, R O, 1998. Mapping chaparral in the Santa Monica Mountains using multiple endmember spectral mixture models. Remote Sens. Environ. 65, 267–279.
Roberts, D A, Dennison, P E, Gardner, M, Hetzel, Y, Ustin, S L, Lee, C, 2003. Evaluation of the potential of Hyperion for fire danger assessment by comparison to the Airborne Visible/Infrared Imaging Spectrometer. IEEE T. Geosci. Remote Sens. 41, 1297–1310.
Roberts, D A, Quattrochi, D A, Hulley, G C, Hook, S J, Green, R O, 2012. Synergies between VSWIR and TIR data for the urban environment: an evaluation of the potential for the hyperspectral infrared imager (HyspIRI) decadal survey mission. Remote Sens. Environ. 117, 83–101.
Roberts, D A, Alonzo, M, Wetherley, E, Dudley, K, Dennison, P, 2017. Multiscale analysis of urban areas using mixing models. In: Quattrochi, D A, Wentz, E, Lam, N S, Emerson, C W (Eds.), Scale in Remote Sensing and GIScience Applications. CRC press, pp. 247–282.
Roberts, D A, Halligan, K, Dennison, P, Dudley, K, Somers, B, Crabbe, A, 2019. Viper Tools User Manual, Version 2.1. (92pp).
Rocha, A V, Shaver, G R, 2011. Postfire energy exchange in arctic tundra: the importance and climatic implications of burn severity. Glob. Chang. Biol. 17, 2831–2841.
Roche, J W, Goulden, M L, Bales, R C, 2018. Estimating evapotranspiration change due to forest treatment and fire at the basin scale in the Sierra Nevada, California. Ecohydrology 11 (7), e1978. doi:10.1002/eco.1978.
Rodriguez-Galiano, V F, Ghimire, B, Rogan, J, Chica-Olmo, M, Rigol-Sanchez, J P, 2012. An assessment of the effectiveness of a random forest classifier for land-cover classification. ISPRS J. Photogramm. Remote Sens. 67, 93–104. doi:10.1016/j.isprsjprs.2011.11.002.
Rogan, J, Franklin, J, 2001. Mapping wildfire burn severity in Southern California forests and shrublands using enhanced Thematic Mapper imagery. Geocarto Int 16, 91–101.
Roth, K L, Dennison, P E, Roberts, D A, 2012. Comparing endmember selection techniques for accurate mapping of plant species and land cover using imaging spectrometer data. Remote Sens. Environ. 127, 139–152.
Rothermel, R C, 1972. A Mathematical Model for Predicting Fire Spread in Wildland Fuels. 40. Intermountain Forest & Range Experiment Station, Forest Service, US Department of Agriculture, Washington, DC.
Roy, D P, Boschetti, L, Trigg, S N, 2006. Remote sensing of fire severity: assessing the performance of the normalized burn ratio. IEEE T. Geosci. Remote Sens. 3, 112–116.
Rubel, F, Brugger, K, Haslinger, K, Auer, I, 2017. The climate of the European Alps: shift of very high resolution Köppen-Geiger climate zones 1800–2100. Meteorol. Z. 26, 115–125.
Sánchez, J M, Kustas, W P, Caselles, V, Anderson, M C, 2008. Modelling surface energy fluxes over maize using a two-source patch model and radiometric soil and canopy temperature observations. Remote Sens. Environ. 112, 1130–1143.
Sánchez, J M, Bisquert, M, Rubio, E, Caselles, V, 2015. Impact of land cover change induced by a fire event on the surface energy fluxes derived from remote sensing. Remote Sensor 7 (11), 14899–14915. doi:10.3390/rs71114899.
San-Miguel-Ayanz, J, Durrant, T, Boca, R, Libertá, G, Branco, A, de Rigo, D, Ferrari, D, Malanti, P, Vivancos, T A, Costa, H, Lana, F, Löffler, P, Nuijten, D, Ahlgren, A C, Leray, T, 2018. Forest Fires in Europe, Middle East and North Africa 2017. EUR 29318 EN. Publications Office, Luxemburg ISBN 978-92-79-92831-4. doi:10.2760/663443.
Schaaf, A N, Dennison, P E, Fryer, G K, Roth, K L, Roberts, D A, 2011. Mapping plant functional types at multiple spatial resolutions using imaging spectrometer data. GIScience Remote Sens 48, 324–344.
Schmidt, A, Niemeyer, J, Rottensteiner, F, Soergel, U, 2014. Contextual classification of full waveform lidar data in the Wadden Sea. IEEE Geosci. Remote Sens. Lett. 11, 1614–1618.
Shakesby, R A, 2011. Post-wildfire soil erosion in the Mediterranean: review and future research directions. Earth-Sci. Rev. 105, 71–100.
Shimabukuro, Y E, Smith, J, 1991. The least-squares mixing models to generatefraction images derived from remote sensing multispectral data. IEEE T. Geosci. Remote 29, 16–21.
Somers, B, Asner, G P, Tits, L, Coppin, P, 2011. Endmember variability in spectral mixture analysis: a review. Remote Sens. Environ. 115, 1603–1616.
Somers, B, Zortea, M, Plaza, A, Asner, G P, 2012. Automated extraction of image-based endmember bundles for improved spectral unmixing. IEEE Journal of Selected Topics in Applied Earth Observations and Remote Sensing, IEEE J-STARS 5, 396–408.
Soverel, N O, Perrakis, D D B, Coops, N C, 2010. Estimating burn severity from Landsat dNBR and RdNBR indices across western Canada. Remote Sens. Environ. 114, 1896–1909.

Stambaugh, M C, Hammer, L D, Godfrey, R, 2015. Performance of burn severity metrics and classification in oak woodlands and grasslands. Remote Sens. 2015 (7), 10501–10522. doi:10.3390/rs70810501.

Storey, M, Price, O, Tasker, E, 2016. The role of weather, past fire and topography in crown fire occurrence in eastern Australia. Int. J. Wildland Fire 25, 1048–1060. doi:10.1071/WF15171.

Tane, Z, Roberts, D, Veraverbeke, S, Casas, A, Ramirez, C, Ustin, S, 2018. Evaluating endmember and band selection techniques for multiple endmember spectral mixture analysis using post-fire imaging spectroscopy. Remote Sens. 10, 389.

Teluguntla, P, Thenkabail, P S, Oliphant, A, Xiong, J, Gumma, M K, Congalton, R G, Yadav, K, Huete, A, 2018. A 30-m landsat-derived cropland extent product of Australia and China using random forest machine learning algorithm on Google Earth Engine cloud computing platform. ISPRS J. Photogramm. Remote Sens. 144, 325–340. doi:10.1016/j.isprsjprs.2018.07.017.

Tompkins, S, Mustard, J F, Pieters, C M, Forsyth, D W, 1997. Optimization of endmembers for spectral mixture analysis. Remote Sens. Environ. 59, 472–489.

Turner, M G, Romme, W H, Gardner, R H, 1999. Prefire heterogeneity, fire severity, and early postfire plant reestablishment in subalpine forests of Yellowstone National Park, Wyoming. Int. J. Wildland Fire 9, 21–36.

van der Tol, C, Norberto-Parodi, G, 2011. Guidelines for remote sensing of evapotranspiration. In: Evapotranspiration. In: Remote sensing and modeling. InTech, Croatia, pp. 227–250.

Veraverbeke, S, Hook, S J, 2013. Evaluating spectral indices and spectral mixture analysis for assessing fire severity, combustion completeness and carbon emissions. Int. J. Wildland Fire 22, 707–720.

Veraverbeke, S, Stavros, E N, Hook, S J, 2014. Assessing fire severity using imaging spectroscopy data from the Airborne Visible/Infrared Imaging Spectrometer (AVIRIS) and comparison with multispectral capabilities. Remote Sens. Environ. 154, 153–163. doi:10.1016/j.rse.2014.08.019.

Veraverbeke, S, Dennison, P, Gitas, I, Hulley, G, Kalashnikova, O, Katagis, T, Kuai, L, Meng, R, Roberts, D, Stavros, N, 2018. Hyperspectral remote sensing of fire: state-of-the-art and future perspectives. Remote Sens. Environ. 216, 105–121.

Viedma, O, Quesada, J, Torres, I, de Santis, A D, Moreno, J M, 2014. Fire severity in a large fire in a Pinus pinaster forest is highly predictable from burning conditions, stand structure, and topography. Ecosystems 18, 237–250.

Wang, H, Zhao, Y, Pu, R, Zhang, Z, 2015. Mapping Robinia pseudoacacia forest health conditions by using combined spectral, spatial, and textural information extracted from IKONOS imagery and random forest classifier. Remote Sens. 7, 9020–9044. doi:10.3390/rs70709020.

Wang, X, Gao, X, Zhang, Y, Fei, X, Chen, Z, Wang, J, Zhang, Y, Lu, X, Zhao, H, 2019. Land-cover classification of coastal wetlands using the RF algorithm for Worldview-2 and Landsat 8 images. Remote Sens. 11, 1927. doi:10.3390/rs11161927.

Wimberly, M C, Reilly, M J, 2007. Assessment of fire severity and species diversity in the southern Appalachians using Landsat TM and ETM + imagery. Remote Sens. Environ. 108, 189–197.

Zhong, L, Gong, P, Biging, G S, 2014. Efficient corn and soybean mapping with temporal extendability: a multi-year experiment using Landsat imagery. Remote Sens. Environ. 140, 1–13.